Electron-Rich Piano-Stool Iron *σ*-Acetylides.† Theoretical and Phenomenological Investigation of Electronic Substituent Effects in Iron(II) Acetylides

Karine Costuas,*,‡ Frédéric Paul,*,§ Loic Toupet,|| Jean-François Halet,‡ and Claude Lapinte§

Organométalliques et Catalyse: Chimie et Electrochimie Moléculaire, UMR CNRS 6509, Groupe Matière Condensée et Matériaux, UMR CNRS 6626, Institut de Chimie de Rennes, and Laboratoire de Chimie du Solide et Inorganique Moléculaire, UMR CNRS 6511, Université de Rennes 1, Campus de Beaulieu, 35042 Rennes Cedex, France

Received October 7, 2003

The electronic structures of the electron-rich Fe(II) acetylide complexes (η^2-dppe)(η^5-C_5Me_5)Fe($C{\equiv}CC_6H_4$-X) (**1a**−**j**: dppe = 1,2-bis(diphenylphosphino)ethane; X = NO_2, CN, CF_3, Br, F, H, Me, ^{t}Bu, OMe, NH_2) have been investigated using density functional theory calculations. The crystal structures of the bromo- (**1d**), methyl- (**1g**), methoxy- (**1i**), and amino-substituted complexes (**1j**) are reported to complement the available structural data. The structural data, the first ionization potentials, and the relevant electronic and vibronic transitions calculated for the model complexes are compared to the experimental data for the corresponding Fe(II) complexes among **1a**−**j**. The influence of the X substituent on the electronic properties is then more specifically investigated by means of linear free-energy relationships (LFERs). Correlations between the experimental data gathered for **1a**−**j** and electronic substituent parameters (ESP's) provide additional information on the way the remote para substituent influences the electronic properties of these Fe(II) acetylide complexes. This dual theoretical/phenomenological approach gives a consistent picture of the bonding between the Fe(II) center and the functional phenylacetylide fragment.

Introduction

Over the past decade organometallic molecular assemblies incorporating metal atoms in organic π-networks have aroused a great deal of interest, owing to the amazing properties that these combinations seem to offer.[2−5] In particular, architectures featuring a central aromatic core exhibit very interesting prospects for the design of new molecular-sized electronic devices.[2q,4,6−15] There is currently a strong need of basic knowledge in this field in order to better delineate structure−property relationships, allowing for the design of new molecular targets best suited to a given goal. More precisely regarding "M−C≡C" units, Manna et al. already pointed out some years ago that "the question of π-interactions between the alkynyl ligand and the metal atom is central to the chemistry and the physical properties of this fragment".[3] In fact, the "capability" of the acetylene bridge to convey magnetic or electronic information is strongly dependent on the interaction occurring between the alkynyl linker and the metal center M in a given redox state, as has now been clearly established by several theoretical and experimental studies.[16−22] To address this question more specifically in the case of electron-rich organoiron acetylides, we have studied the family of Fe(II) and Fe(III) [(η^2-

† For previous contributions on similar Fe(II) and Fe(III) alkynyls, see ref 1.

‡ Laboratoire de Chimie du Solide et Inorganique Moléculaire, UMR CNRS 6511.

§ Organométalliques et Catalyse: Chimie et Electrochimie Moléculaire, UMR CNRS 6509.

|| Groupe Matière Condensée et Matériaux, UMR CNRS 6626.

(1) (a) Denis, R.; Toupet, L.; Paul, F.; Lapinte, C. *Organometallics* **2000**, *19*, 4240−4251. (b) Paul, F.; Mevellec, J.-Y.; Lapinte, C. *Dalton* **2002**, 1783−1790. (c) Paul, F.; Costuas, K.; Ledoux, I.; Deveau, S.; Zyss, J.; Halet, J.-F.; Lapinte, C. *Organometallics* **2002**, *21*, 5229−5235. (d) Courmarcel, J.; Le Gland, G.; Toupet, L.; Paul, F.; Lapinte, C. *J. Organomet. Chem.* **2003**, *670*, 108−122. (e) Paul, F.; Lapinte, C. Work in progress.

(2) For some relevant reviews, see: (a) Chisholm, M. H. *Angew. Chem., Int. Ed. Engl.* **1991**, *30*, 673−674. (b) Beck, W.; Niemer, B.; Wieser, M. *Angew. Chem., Int. Ed. Engl.* **1993**, *32*, 923−949. (c) Lang, H. *Angew. Chem., Int. Ed. Engl.* **1994**, *33*, 547−550. (d) Akita, M.; Moro-Oka, Y. *Bull. Chem. Soc. Jpn.* **1995**, *68*, 420−432. (e) Long, N. J. *Angew. Chem., Int. Ed. Engl.* **1995**, *34*, 21−38. (f) Ward, M. D. *Chem. Ind.* **1996**, 568−573. (g) Bunz, U. H. F. *Angew. Chem., Int. Ed. Engl.* **1996**, *35*, 969−971. (h) Barigelletti, F.; Flamigni, L.; Collin, J.-P.; Sauvage, J.-P. *Chem. Commun.* **1997**, 333−338. (i) Bruce, M. I. *Coord. Chem. Rev.* **1997**, *166*, 91−119. (j) Ziessel, R.; Hissler, M.; El-gayhouri, A.; Harriman, A. *Coord. Chem. Rev.* **1998**, *178−180*, 1251−1298. (k) Whittall, I. R.; MacDonagh, A. M.; Humphrey, M. G.; Samoc, M. *Adv. Organomet. Chem.* **1998**, *42*, 291−362. (l) Whittall, I. R.; MacDonagh, A. M.; Humphrey, M. G.; Samoc, M. *Adv. Organomet. Chem.* **1998**, *43*, 349−322. (m) Yam, V. W.-W.; Lo, K. K.-W.; Wong, K. M.-C. *J. Organomet. Chem.* **1999**, *578*, 3−30. (n) Schwab, P. F. H.; Levin, M. D.; Michl, J. *Chem. Rev.* **1999**, *99*, 1863−1933. (o) Martin, R. E.; Diederich, F. *Angew. Chem., Int. Ed.* **1999**, *38*, 1351−1377. (p) Ziessel, R. *Synthesis* **1999**, 1839−1865. (q) Yam, V. W.-W. *Acc. Chem. Res.* **2002**, *35*, 555−563.

(3) Manna, J.; John, K. D.; Hopkins, M. D. *Adv. Organomet. Chem.* **1995**, *38*, 80−154.

(4) (a) Paul, F.; Lapinte, C. *Coord. Chem. Rev.* **1998**, *178/180*, 427−505. (b) Paul, F.; Lapinte, C. In *Unusual Structures and Physical Properties in Organometallic Chemistry*; Gielen, M., Willem, R., Wrackmeyer, B., Eds.; Wiley: San Francisco, CA, 2002; pp 219−295.

(5) Dembinski, R.; Bartik, T.; Bartik, B.; Jaeger, M.; Gladysz, J. A. *J. Am. Chem. Soc.* **2000**, *122*, 810−822 and references cited therein.

(6) Köhler, F. H.; Prössdorf, W.; Schubert, U. *Inorg. Chem.* **1981**, *20*, 4096−4101.

(7) (a) Werner, H.; Rappert, T.; Wolf, J. *Isr. J. Chem.* **1990**, *30*, 377−384. (b) Werner, H.; Bachmann, P.; Laubender, M.; Gevert, O. *Eur. J. Inorg. Chem.* **1998**, 1217−1207.

10.1021/om030630k CCC: $27.50
Publication on Web 03/23/2004

dppe)(η^5-C_5Me_5)Fe(C≡CC_6H_4X)]$^{n+}$(PF_6)$_n^-$ complexes (**1a**−**j**, n = 0; **1a**$^+PF_6^-$−**1j**$^+PF_6^-$, n = 1; dppe = 1,2-bis(diphenylphosphino)ethane).

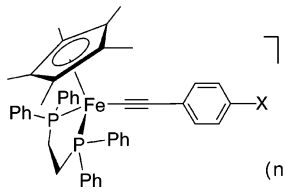

X	
1a: NO_2	**1g**: Me
1b: CN	**1h**: ^{t}Bu
1c: CF_3	**1i**: OMe
1d: Br	**1j**: NH_2
1e: F	
1f: H	

The first paper dealing with this topic was devoted to the synthesis and characterization of these complexes.[1a] The electronic influence of the X substituent on the alkynyl bridge was then studied by means of vibrational spectroscopy and electric field induced second harmonic generation (EFISH).[1b,c] Infrared (IR) spectroscopy clearly evidenced the decisive electronic influence of X on the bond order and on the local polarization of the alkynyl unit.[1b] The importance of mesomeric factors was suggested by linear free energy relationships (LFERs) involving IR data. Thus, considering the simple valence bond (VB) scheme that was initially proposed as a working hypothesis to rationalize the structural influence of the substituent in Fe(II) complexes (Scheme 1),[1a] these contributions have further evidenced the decisive role of B in the VB description.[1b]

Scheme 1

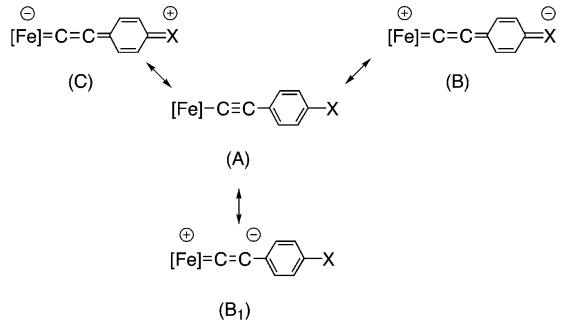

To refine this VB description and also to better understand the electronic substituent effect in the vicinity of the iron center, a density functional theory (DFT) study was conducted on several [(PH_3)$_2$(η^5-C_5H_5)-Fe(C≡CC_6H_4X)]$^{n+}$(PF_6^-)$_n$ model complexes (**1a**-H/**1a**-H$^+PF_6^-$ to **1j**-H/**1j**-H$^+PF_6^-$) with varied substituents (n = 0, 1; X = NO_2, CN, Br, H, OMe, NH_2). We have also pursued our phenomenological investigation of the substituent effect by correlating other characteristic thermodynamic or spectroscopic data of Fe(II) acetylides **1a**−**j** with electronic substituent parameters (ESPs).[23,24] The new LFERs obtained reveal in an *empirical* way the significant substituent effects operative on remote parts of the molecule. They usefully complement the theoretical study for analyzing the electronic communication between the metal and the X substituent in these electron-rich Fe(II) acetylides. Such an understanding constitutes an important issue for the design of new molecular devices based on the "Fe−C≡C" fragment.

Results

X-ray Structures of (η^2-dppe)(η^5-C_5Me_5)Fe(C≡C)-1,4-(C_6H_4)X Complexes with X = Br (1d), Me (1g), OMe (1i), NH_2 (1j). Complexes **1d**,**g** crystallize in the triclinic space group with two molecules in the asymmetric unit, while **1i**,**j** crystallize in the monoclinic space group with four molecules in the asymmetric unit (Figures 1−4 and Table 1). Both crystalline arrangements have previously been observed for analogous Fe(II) complexes.[1a,d] The bond distances and angles (Table 2) in the coordination sphere of the metal center appear

(8) (a) Davies, S. J.; Johnson, B. F. G.; Lewis, J.; Khan, M. S. *J. Organomet. Chem.* **1991**, *401*, C43−C45. (b) Colbert, M. C. C.; Lewis, J.; Long, N. J.; Raithby, P. R.; Younus, M.; White, A. J. P.; Williams, D. J.; Payne, N. J.; Yellowlees, L.; Beljonne, D.; Chawdhury, N.; Friend, R. H. *Organometallics* **1998**, *17*, 3034−3043. (c) Younus, M.; Long, N. J.; Raithby, P. R.; Lewis, J. *J. Organomet. Chem.* **1998**, *570*, 55−62.
(9) Tykwinski, R.; Stang, P. J. *Organometallics* **1992**, *13*, 3203−3208.
(10) Long, N. J.; Martin, A. J.; de Biani, F. F.; Zanello, P. *J. Chem. Soc., Dalton Trans.* **1998**, 2017−2021.
(11) Uno, M.; Dixneuf, P. H. *Angew. Chem., Int. Ed.* **1998**, *37*, 1714−1717.
(12) Bruce, M. I.; Hall, B. C.; Low, P. J.; Skelton, B. W.; White, A. H. *J. Organomet. Chem.* **1999**, *592*, 74−83.
(13) (a) MacDonagh, A. R.; Humphrey, M. G.; Samoc, M.; Luther-Davies, B.; Houbrechts, S.; Wada, T.; Sasabe, H.; Persoons, A. *J. Am. Chem. Soc.* **1999**, *121*, 1405−1406. (b) MacDonagh, A. R.; Humphrey, M. G.; Samoc, M.; Luther-Davies, B. *Organometallics* **1999**, *18*, 5195−5197.
(14) John, K. D.; Hopkins, M. D. *Chem. Commun.* **1999**, 589−590.
(15) (a) Le Narvor, N.; Lapinte, C. *Organometallics* **1995**, *14*, 634−639. (b) Weyland, T.; Lapinte, C.; Frapper, G.; Calhorda, M. J.; Halet, J.-F.; Toupet, L. *Organometallics* **1997**, *16*, 2024−2031. (c) Weyland, T.; Costuas, K.; Mari, A.; Halet, J.-F.; Lapinte, C. *Organometallics* **1998**, *17*, 5569−5579. (d) Weyland, T.; Costuas, K.; Toupet, L.; Halet, J.-F.; Lapinte, C. *Organometallics* **2000**, *19*, 4228−4239. (e) Weyland, T.; Ledoux, I.; Brasselet, S.; Zyss, J.; Lapinte, C. *Organometallics* **2000**, *19*, 5235−5237.
(16) Kostic, N. M.; Fenske, R. F. *Organometallics* **1982**, *1*, 974−982.
(17) (a) Lichtenberger, D. L.; Renshaw, S. K.; Bullock, R. M. *J. Am. Chem. Soc.* **1993**, *115*, 3276−3285. (b) Lichtenberger, D. L.; Renshaw, S. K. *Organometallics* **1993**, *12*, 3522−3526. (c) Lichtenberger, D. L.; Gruhn, N. E.; Renshaw, S. K. *J. Mol. Struct.* **1997**, *405*, 79−86.
(18) (a) de Angelis, F.; Re, N.; Rosi, M.; Sgamellotti, A.; Floriani, C. *J. Chem. Soc., Dalton Trans.* **1997**, 3841−3844. (b) Belanzoni, P.; Re, N.; Sgamellotti, A.; Floriani, C. *J. Chem. Soc., Dalton Trans.* **1998**, 1825−1835. (c) Belanzoni, P.; Re, N.; Rosi, M.; Sgamellotti, A.; Floriani, C. *Organometallics* **1996**, *15*, 4264−4273.
(19) (a) MacGrady, J. E.; Lovell, T.; Stranger, R.; Humphrey, M. G. *Organometallics* **1997**, *16*, 4004−4011. (b) Delfs, C. D.; Stranger, R.; Humphrey, M. G.; MacDonagh, A. M. *J. Organomet. Chem.* **2000**, *607*, 208−212. (c) Powell, C. E.; Cifuentes, M. P.; McDonagh, A. M.; Hurst, S. K.; Lucas, N. T.; Delfs, C. D.; Stranger, R.; Humphrey, M. G.; Houbrechts, S.; Asselberghs, I.; Persoons, A.; Hockless, D. C. R. *Inorg. Chim. Acta* **2003**, *352*, 9−18.
(20) (a) Low, P. J.; Rousseau, R.; Lam, P.; Udachin, K. A.; Enright, G. D.; Tse, J. S.; Wayner, D. D. M.; Carty, A. J. *Organometallics* **1999**, *18*, 3885−3897. (b) Koentjoro, O. F.; Rousseau, R.; Low, P. J. *Organometallics* **2001**, *20*, 4502−4509.
(21) To our knowledge, the only other contribution dealing with related Hammett correlations on transition-metal−σ-acetylide complexes was published during the reviewing process of the present paper: Hurst, S. K.; Xu, G.-L.; Ren, T. *Organometallics* **2003**, *22*, 4118−4123.
(22) Related investigations on dinuclear acetylide complexes stable under several redox states: (a) Le Narvor, N.; Toupet, L.; Lapinte, C. *J. Am. Chem. Soc.* **1995**, *117*, 7129−7138. (b) Brady, M.; Weng, W.; Zhou, Y.; Seyler, J. W.; Amoroso, A. J.; Arif, A. M.; Böhme, M.; Frenking, G.; Gladysz, J. A. *J. Am. Chem. Soc.* **1997**, *119*, 775−788. (c) Kheradmandan, S.; Heinze, K.; Schmalle, H.; Berke, H. *Angew. Chem., Int. Ed. Engl.* **1979**, *18*, 2270−2273. (d) Bruce, M. I.; Low, P. J.; Costuas, K.; Halet, J.-F.; Best, S. P.; Heath, G. H. *J. Am. Chem. Soc.* **2000**, *122*, 1949−1962. (e) Paul, F.; Meyer, W.; Jiao, H.; Toupet, L.; Gladysz, J. A.; Lapinte, C. *J. Am. Chem. Soc.* **2000**, *122*, 9405−9414. (f) Jiao, H.; Gladysz, J. A. *New J. Chem.* **2001**, *25*, 551−562. (g) Jiao, H.; Gladysz, J. A.; Costuas, K.; Halet, J.-F.; Toupet, L.; Paul, F.; Lapinte, C. *J. Am. Chem. Soc.* **2003**, *125*, 9511−9522. (h) Bruce, M. I.; Ellis, B. G.; Low, P. J.; Skelton, B. W.; White, A. H. *Organometallics.* **2003**, *22*, 3184−3198.
(23) Jaffé, H. H. *Chem. Rev.* **1953**, *53*, 191−261.
(24) de Courville, A.; Peltier, D. *Bull. Soc. Chim. Fr.* **1967**, 2164−2167.

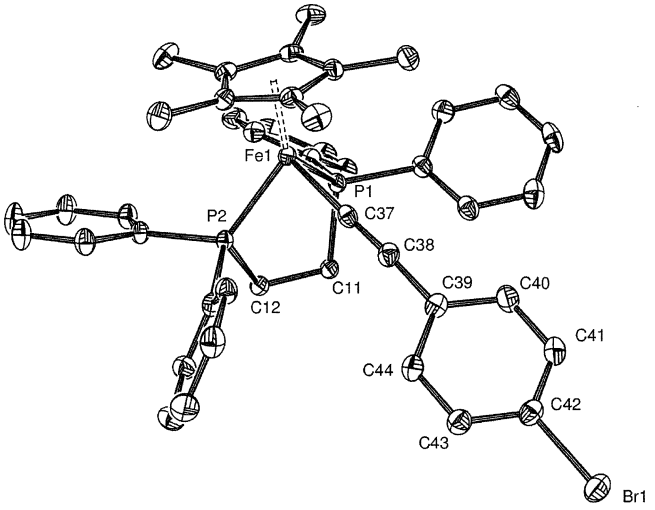

Figure 1. Molecular structure of (η^2-dppe)(η^5-C_5Me_5)Fe-(C≡C)-1,4-(C_6H_4)Br (**1d**).

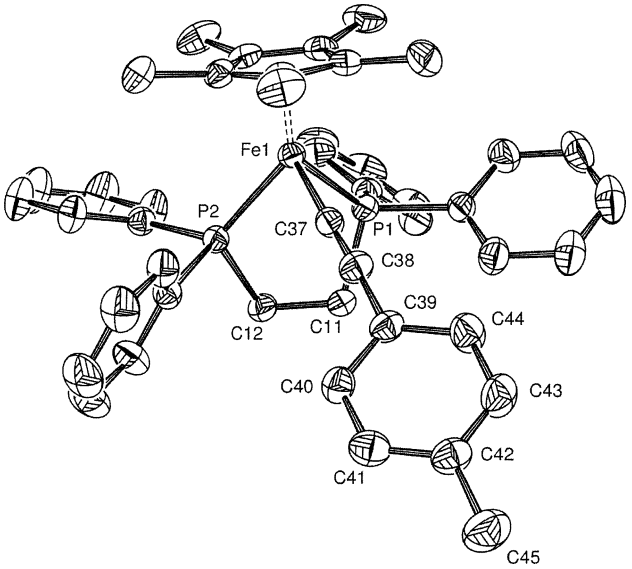

Figure 2. Molecular structure of (η^2-dppe)(η^5-C_5Me_5)Fe-(C≡C)-1,4-(C_6H_4)Me (**1g**).

comparable to those commonly encountered in related piano-stool complexes.[1a,d,25] For the 1,4-bromo-, 4-tolyl-, 1,4-methoxy-, and 1,4-aminophenylethynyl ligands, the triple-bond lengths are in the expected range (i.e. 1.210 Å).[3] Considering the experimental standard deviations (esds), the bond distances of all complexes compare to those of the unsubstituted complex **1f**·C_5H_{12} (X = H),[1] especially the Fe−C37 bond as well as the C38−C39 bond (1.894 and 1.430 Å, respectively). Bending of the C37−C38−C39 axis (174.8, 175.8, 176.6, and 177.2° in **1d**,**g**,**i**,**j,** respectively) has also previously been observed with electron-withdrawing substituents.[1a] Concerning the X substituents, the complexes **1d**,**g** have classical bond distances between C42 and X.[26] Regarding the corresponding bond in **1i**, the coplanarity of the aryl and methoxy substituents (dihedral angle of 3.9°) suggests some conjugation with the ring. However, the slightly

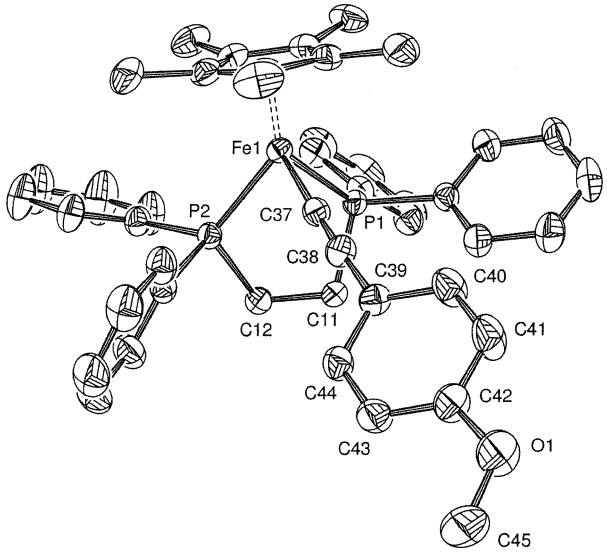

Figure 3. Molecular structure of (η^2-dppe)(η^5-C_5Me_5)Fe-(C≡C)-1,4-(C_6H_4)OCH_3 (**1i**).

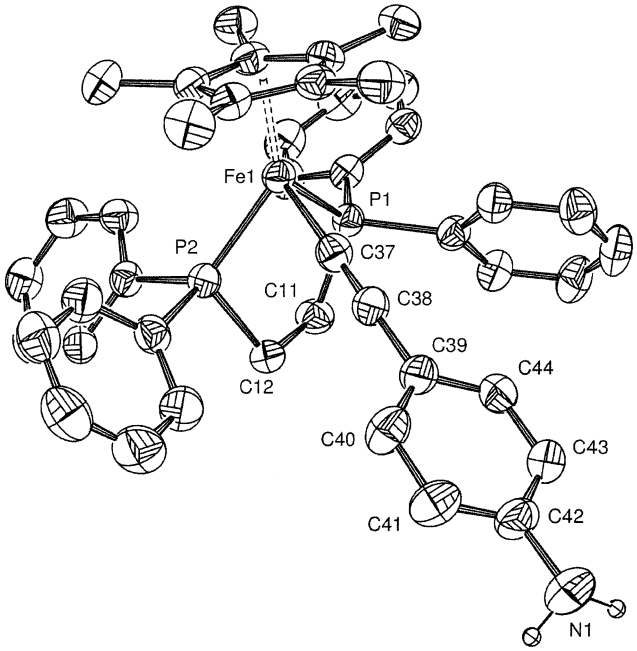

Figure 4. Molecular structure of (η^2-dppe)(η^5-C_5Me_5)Fe-(C≡C)-1,4-(C_6H_4)NH_2 (**1j**).

longer C42−O1 (and significantly shorter C45−O1) bond distances relative to their expected mean values (1.382/1.383 Å vs 1.370/1.424 Å, respectively) indicate a dominantly repulsive interaction between these fragments.[26] A similar statement can also be made for the C42−X bond in **1j**. Despite the apparent coplanarity between the amino mean plane and the phenyl ring, the C42−N1 distance is slightly longer than usually observed for sp^2-hybridized amino substituents (1.406 Å vs 1.394 Å).[26]

Theoretical Study of the Model Complex Series [$(PH_3)_2(\eta^5$-$C_5H_5)$Fe(C≡CC_6H_4X)]$^{n+}$(PF_6^-)$_n$. A careful analysis of the metal−ligand interactions in the [$(PH_3)_2$-(η^5-C_5H_5)Fe(C≡CC_6H_4X)]$^{n+}$(PF_6^-)$_n$ series (n = 0, 1; X = NO_2, CN, Br, H, OMe, NH_2) is necessary to understand the influence of the X substituent on the properties of the molecule.

(25) Garcia, M. H.; Robalo, M. P.; Dias, A. R.; Duarte, M. T.; Weenseleers, W.; Aerts, G.; Govaerts, E.; Cifuentes, M. P.; Hurst, S.; Humphrey, M. G.; Samoc, M.; Luther-Davies, B. *Organometallics* **2002**, *21*, 2107−2118.

(26) Allen, F. H.; Kennard, O.; Watson, D. G.; Brammer, L.; Orpen, A. G.; Taylor, R. *J. Chem. Soc., Perkin Trans.* **1987**, *2*, S1−S19.

Table 1. Crystal Data, Data Collection Details, and Refinement Parameters for 1d,g,i,j

	1d (X = Br)	**1g** (X = Me)	**1i** (X = OMe)	**1j** (X = NH_2)
formula	$C_{44}H_{43}BrP_2Fe$	$C_{45}H_{46}P_2Fe$	$C_{45}H_{46}OP_2Fe$	$C_{44}H_{45}NP_2Fe$
fw	769.48	704.61	720.61	705.60
temp (K)	293(2)	293(2)	293(2)	293(2)
cryst syst	triclinic	triclinic	monoclinic	monoclinic
space group	$P\bar{1}$	$P\bar{1}$	$P2_1/n$	$P2_1/c$
a (Å)	12.0396(3)	12.1178(2)	12.0199(2)	15.4172(4)
b (Å)	12.2007(3)	12.3138(2)	19.9019(3)	11.0980(3)
c (Å)	15.2532(5)	15.4522(4)	16.0099(3)	22.3218(7)
α (deg)	72.8200(10)	73.213(1)	90.00	90.00
β (deg)	70.8570(10)	71.294(1)	91.7285(6)	107.535(1)
γ (deg)	61.2860(10)	61.120(1)	90.00	90.00
V (Å^{-3})	1830.52(9)	1887.22(7)	3828.13(11)	3641.8(2)
Z	2	2	4	4
D_{calcd} (g cm^{-3})	1.396	1.204	1.250	1.287
cryst size (mm)	0.22 × 0.18 × 0.18	0.42 × 0.18 × 0.16	0.32 × 0.21 × 0.21	0.35 × 0.22 × 0.20
F(000)	796	744	1520	1488
diffractometer (NONIUS)	Kappa CCD	Kappa CCD	Kappa CCD	Kappa CCD
radiation	Mo Kα	Mo Kα	Mo Kα	Mo Kα
abs coeff (mm^{-1})	1.622	0.515	0.511	0.534
$2\theta_{max}$ (deg)	54	54	60	54
no. of frames	147	162	145	130
Ω rotation (deg)	2.0	2.0	1.7	1.5
rate (s/frame)	400	40	34	75
θ range (deg)	2.07−27.52	1.41−27.49	2.05−27.48	2.00−27.53
hkl range	0−15, −13 to +15, −18 to +19	0−15, −13 to +15, −18 to +20	0−15, 0−25, −20 to +20	0−20, 0−14, −28 to +27
total no. of rflns	8347	8618	8761	8371
no. of unique rflns	8347	8618	8761	8371
no. of obsd rflns ($I > 2\sigma(I)$)	6582	6120	6755	4907
no. of restraints/params	0/434	0/434	0/443	0/440
a[a]	0.0469	0.0958	0.0584	0.0875
b[a]	4.9859	0.2134	1.6870	0.7416
final R	0.0516	0.0516	0.0431	0.055
R_w	0.1243	0.1395	0.1105	0.140
R indices (all data)	0.0741	0.0820	0.0633	0.1175
R_w (all data)	0.1380	0,1618	0.1219	0.1730
goodness of fit/F^2 (S_w)	1.063	1.019	1.045	1.005
$\Delta\rho_{max}$ (e Å^{-3})	0.67	0.46		0.62
largest diff peak, hole (e Å^{-3})	0.676, −0.688	0.466, −0.416	0.372, −0.393	0.618, −0.368

[a] $w = 1/[\sigma^2(F_o)^2 + (aP)^2 + bP]$ (where $P = [F_o^2 + F_c^2]/3$).

1. Qualitative Analysis. The schematic extended Hückel (EH) description of the interaction between $[(Cp)(L)_2Fe]^+$ and $[C{\equiv}CPh]^-$ fragments (Cp = η^5-C_5H_5, L = PH_3) is illustrated in Figure 5. The pseudo-octahedral $[(Cp)(L)_2Fe]^+$ fragment possesses four frontier molecular orbitals (FMOs) susceptible to interact with the organic moiety: one vacant σ-type orbital (3a′), and three occupied d-type FMOs (1a′, 1a″, 2a′) related to the t_{2g} orbital set of an octahedral ML_6 system (see the left-hand side of Figure 5).[27] The latter set of orbitals is composed of two nearly degenerated π-type orbitals, $\pi_\perp$ and $\pi_\parallel$, and a δ-type orbital. The FMOs of the $[C{\equiv}CPh]^-$ fragment are given on the right-hand side of Figure 5. Six among them interact with the metallic fragment: two nondegenerate occupied π-type orbitals, $\pi_\parallel$ (1a″) and $\pi_\perp$ (1a′), a σ-type orbital (2a′), and three vacant π^* orbitals (3a′, 4a″, and 4a′). The bonding between the metallic moiety and the arylacetylide fragment is mainly governed by a strong σ-type interaction between the high-lying σ FMO of the metallic fragment (3a′) and the occupied FMO of the organic moiety of the corresponding symmetry (2a′). This leads to a strong donation from the arylacetylide toward the metal center. This interaction is augmented by a weaker π donation mainly from the two π-type metallic FMOs, 1a″ ($\pi_\parallel$) and 2a′ ($\pi_\perp$), to the π^* FMOs of the C≡CR fragment (3a′, 4a′ ($\pi_\perp^*$), and 4a″ ($\pi_\parallel^*$) respectively), as shown in Figure 5. The highest occupied molecular orbital (HOMO) of $(Cp)(L)_2Fe(C{\equiv}CPh)$ mainly results from the antibonding combination of the former with occupied FMOs of the acetylide ligand. It is roughly equally delocalized over the Fe atom and the carbon atoms of the arylacetylide ligand.

The presence of a para substituent X on the aryl ring slightly modifies the electronic structure of the molecule, stabilizing or destabilizing the HOMOs. To analyze this electronic influence, the DFT FMOs of the $[C{\equiv}CC_6H_4X]^-$ fragments (X = NO_2, CN, Br, H, OMe, NH_2) were computed (Figure 6). The major effect of this substitution is a destabilization of the FMOs as the electron-releasing character of the substituent increases (from NO_2 to NH_2). Consequently, both the π and σ framework of the entire molecule $(PH_3)_2(\eta^5\text{-}C_5H_5)Fe(C{\equiv}CC_6H_4X)$ are affected. For X = NO_2, an extra nonbonding MO (28a; see the left-hand side of Figure 6) is also added to the FMO set previously described for the C≡CPh fragment.

2. DFT-Optimized Geometries and Electronic Structures of the $[(\eta^2\text{-dppe})(\eta^5\text{-}C_5Me_5)Fe(C{\equiv}CC_6H_4X)]^{n+}(PF_6^-)_n$ Series (n = 0, 1; X = NO_2, CN, Br, H, OMe, NH_2). The geometries of the model complexes **1a**-H, **1b**-H, **1d**-H, **1f**-H, **1i**-H, and **1j**-H and their corresponding radical cations **1a**-H^+, **1b**-H^+, **1d**-H^+, **1f**-H^+, **1i**-H^+, and **1j**-H^+ were optimized. These optimizations were carried out without any symmetry constraint (see the Experimental Section). The calculated bond distances for $[(H_3P)_2(\eta^5\text{-}C_5H_5)Fe(C{\equiv}CC_6H_4X)]^{n+}(PF_6^-)_n$ models (n = 0, 1; X = NO_2, CN, Br, H, OMe, NH_2) are

(27) Schilling, B. E. R.; Hoffmann, R.; Lichtenberger, D. L. *J. Am. Chem. Soc.* **1979**, *101*, 585−591.

Table 2. Selected Bond Lengths (Å) and Angles (deg) for 1d,g,i,j

	1d (X = Br)	**1g** (X = Me)	**1i** (X = OMe)	**1j** (X = NH_2)
		Bond Lengths		
Fe−Cp*$_{centroid}$	1.738	1.738	1.740	1.745
Fe−P1	2.1805(10)	2.1829(8)	2.1789(6)	2.1843(10)
Fe−P2	2.1906(10)	2.1924(7)	2.1884(6)	2.1875(10)
Fe−C37	1.898(4)	1.896(3)	1.899(2)	1.916(4)
C37−C38	1.222(5)	1.220(4)	1.215(3)	1.216(5)
C38−C39	1.440(5)	1.440(4)	1.437(3)	1.439(5)
C39−C40	1.408(5)	1.400(4)	1.383(3)	1.387(5)
C40−C41	1.389(5)	1.373(4)	1.378(4)	1.389(5)
C41−C42	1.379(6)	1.375(4)	1.377(4)	1.374(6)
C42−C43	1.394(5)	1.381(5)	1.383(3)	1.392(6)
C43−C44	1,393(5)	1.376(5)	1.387(3)	1.373(5)
C44−C39	1.405(5)	1.404(4)	1.389(3)	1.394(5)
C42−Br1	1.904(4)			
C42−C45		1.512(4)		
C42−O1			1.382(3)	
C45−O1			1.383(4)	
C42−N1				1.406(5)
		Bond Angles		
P1−Fe−P2	86.36(4)	86.25(3)	86.50(2)	85.87(4)
P1−Fe−C37	83.08(10)	82.91(8)	82.37(7)	86.74(11)
P2−Fe−C37	86.69(11)	86.03(8)	86.30(7)	80.20(11)
Fe−C37−C38	177.9(3)	178.7(3)	178.1(2)	177.2(3)
C37−C38−C39	174.8(4)	175.8(3)	176.6(2)	172.8(4)
C40−C39−C44	117.2(3)	116.5(3)	116.8(2)	115.8(3)
C41−C42−C43	120.9(3)	116.9(3)	119.7(2)	118.7(2)
C41−C42−Br1	120.4(3)			
C43−C42−Br1	118.6(3)			
C41−C42−C45		120.9(3)		
C43−C42−C45		122.2(3)		
C41−C42−O1			115.7(2)	
C43−C42−O1			124.6(2)	
C42−O1−C45			118.9(2)	
C41−C42−N1				121.2(4)
C43−C42−N1				120.8(4)
Fe−Cp*$_{centroid}$/ C39−C40[a]	83.5	77.4	−65.4	105.9

[a] Dihedral angle (Cp* = pentamethylcyclopentadienyl ligand).

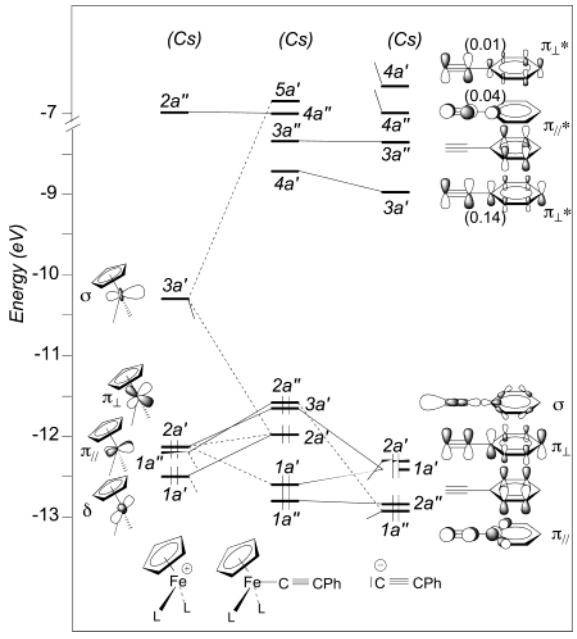

Figure 5. EH interaction diagram between the frontier orbitals of the $[(PH_3)_2(\eta^5\text{-}C_5H_5)Fe]^+$ and the $[(C{\equiv}C)\text{-}1,4\text{-}(C_6H_5)]^-$ fragments.

reported in Table 3, using the numbering shown in Chart 1, and compared to the available X-ray data of several $[(\eta^2\text{-dppe})(\eta^5\text{-}C_5Me_5)Fe(C{\equiv}CC_6H_4X)]^{n+}$ complexes (see the Discussion).[1a,d,e]

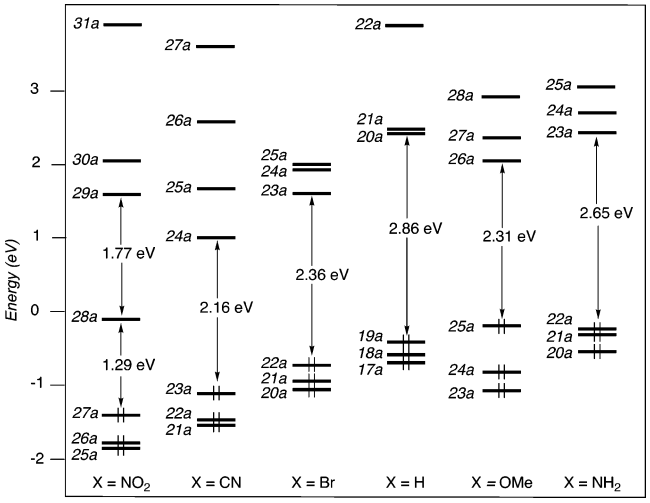

Figure 6. Energy (eV) of the frontier orbitals of the $[(C{\equiv}C)\text{-}1,4\text{-}(C_6H_4)X]^-$ fragment (X = NO_2, CN, Br, H, OMe, NH_2).

The atomic composition of the MOs of Fe(II) acetylides is given in Table 4. In accordance with the preliminary qualitative analysis (Figure 5), the first two HOMOs are localized on the metal−arylacetylide framework. These are shown in Figure 7 for X = NO_2 (**1a**-H) and NH_2 (**1j**-H). The HOMOs of the **1a**-H, **1b**-H, **1d**-H, and **1f**-H Fe(II) acetylides possess a strong iron and acetylide β-carbon character (ca. 60% and 22%, respectively). They correspond to the 2a″ ($\pi_{\|}$) MO of the qualitative diagram shown in Figure 5. For **1i**-H and **1j**-H, the 3a′ ($\pi_{\perp}$) MO (see Figure 5) becomes the HOMO of the system and shows a larger phenyl and X character (see Table 4). For all of the systems except X = NO_2, the LUMO is an Fe−Cp antibonding orbital (corresponding to the 4a″ MO of the qualitative diagram shown in Figure 5). With X = NO_2 (**1a**-H), the corresponding MO is LUMO-1, which is 0.13 eV higher in energy than the LUMO and is localized on the aryl−NO_2 moiety.[28]

With the exception of the NO_2-containing complex **1a**-H, the HOMO−LUMO gap slightly decreases as the substituent becomes more electron-releasing (Figure 8 and Table 5). This exception is due to an NO_2 ligand orbital which inserts between the HOMO and the first antibonding vacant orbital. This peculiar structure might impart slightly different optical properties to **1a** with respect to the rest of the series.[29] As expected, with the more electron donating substituents (X = OMe, NH_2), the HOMO is slightly destabilized with respect to the other substituents, leading to a smaller HOMO−LUMO gap.

Chart 1

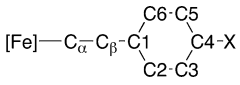

(28) The theoretical study of the model complex **1a**-H with the (4-nitrophenyl)alkynyl ligand in a different conformation (i.e. perpendicular to the Cp plane) and with an imposed C_s symmetry has recently been reported: the different conformation and symmetry apparently leads to slightly different electronic transition energies.[19c]

(29) Barlow, S.; Bunting, H. E.; Ringham, C.; Green, J. C.; Bublitz, G. U.; Boxer, S. G.; Perry, J. W.; Marder, S. R. *J. Am. Chem. Soc.* **1999**, *121*, 3715−3723.

Table 3. Selected Bond Distances (Å) Computed for $[(PH_3)_2(\eta^5\text{-}C_5H_5)Fe(C{\equiv}CC_6H_4\text{-}X)]^{n+}(PF_6^-)_n$ Compared to the X-ray Data Available for the $[(\eta^2\text{-dppe})(\eta^5\text{-}C_5Me_5)Fe(C{\equiv}CC_6H_4X)]^{n+}(PF_6^-)_n$ Complexes (n = 0, 1; X = NO_2, CN, Br, H, OMe, NH_2)[a]

	1a-H	**1a**-H^+	**1b**-H	**1b**-H^+
X	NO_2	NO_2	CN	CN
Fe−C_a	1.89 (1.88)	1.85 (1.89)	1.89 (1.88)	1.85 (1.89)
C_a−C_b	1.24 (1.22)	1.24 (1.21)	1.24 (1.22)	1.25 (1.22)
C_b−C1	1.42 (1.42)	1.42 (1.44)	1.42 (1.43)	1.42 (1.44)
C1−C2	1.42 (1.41)	1.41 (1.39)	1.42 (1.39)	1.42 (1.40)
C2−C3	1.38 (1.36)	1.39 (1.38)	1.39 (1.36)	1.38 (1.38)
C3−C4	1.40 (1.37)	1.39 (1.36)	1.41 (1.39)	1.41 (1.40)
C4−C5	1.40 (1.37)	1.39 (1.36)	1.41 (1.38)	1.41 (1.40)
C5−C6	1.39 (1.37)	1.39 (1.38)	1.39 (1.37)	1.38 (1.39)
C6−C1	1.42 (1.39)	1.41 (1.39)	1.42 (1.41)	1.42 (1.40)
Fe−Cp[b]	1.75 (1.74)	1.79 (1.79)	1.74 (1.74)	1.79 (1.77)
Fe−P	2.26 (2.19)	2.31 (2.24)	2.26 (2.19)	2.33 (2.25)
	2.26 (2.18)	2.31 (2.26)	2.26 (2.18)	2.31 (2.27)
C4−X	1.46 (1.45)	1.48 (1.47)	1.43 (1.44)	1.43 (1.43)
δ[c]	90 (116)	90 (90)	90 (109)	86 (90)
	1d-H	**1d**-H^+	**1f**-H	**1f**-H^+ [d]
X	Br	Br	H	H
Fe−C_a	1.91 (1.90)	1.85 (1.88)	1.91 (1.89)	1.85 (1.92)
C_a−C_b	1.24 (1.22)	1.25 (1.23)	1.24 (1.21)	1.25 (1.21)
C_b−C1	1.42 (1.44)	1.41 (1.43)	1.43 (1.43)	1.41 (1.44)
C1−C2	1.42 (1.41)	1.42 (1.41)	1.41 (1.38)	1.42 (1.41)
C2−C3	1.39 (1.39)	1.39 (1.38)	1.39 (1.38)	1.39 (1.34)
C3−C4	1.39 (1.38)	1.40 (1.38)	1.40 (1.34)	1.40 (1.39)
C4−C5	1.39 (1.39)	1.40 (1.39)	1.40 (1.36)	1.40 (1.38)
C5−C6	1.39 (1.39)	1.39 (1.38)	1.39 (1.38)	1.39 (1.40)
C6−C1	1.41 (1.40)	1.42 (1.40)	1.41 (1.38)	1.42 (1.36)
Fe−Cp[b]	1.74 (1.74)	1.78 (1.78)	1.74 (1.74)	1.78 (1.77)
Fe−P	2.26 (2.19)	2.29 (2.25)	2.26 (2.17)	2.28 (2.25)
	2.26 (2.18)	2.32 (2.26)	2.26 (2.19)	2.31 (2.26)
C4−X	1.95 (1.90)	1.92 (1.90)	1.09	1.09
δ[c]	90 (83)	85 (90)	90 (111)	92 (41)
	1i-**H**	1i-**H**$^+$	**1j**-H	**1j**-H^+
X	OMe	OMe	NH_2	NH_2
Fe−C_a	1.91 (1.90)	1.85 (1.89)	1.91 (1.92)	1.84 (1.86)
C_a−C_b	1.24 (1.21)	1.25 (1.22)	1.24 (1.22)	1.25 (1.22)
C_b−C1	1.43 (1.44)	1.40 (1.44)	1.43 (1.44)	1.40 (1.43)
C1−C2	1.41 (1.38)	1.42 (1.41)	1.41 (1.39)	1.43 (1.41)
C2−C3	1.39 (1.38)	1.37 (1.38)	1.39 (1.37)	1.38 (1.38)
C3−C4	1.40 (1.38)	1.41 (1.40)	1.41 (1.39)	1.42 (1.39)
C4−C5	1.40 (1.38)	1.41 (1.39)	1.40 (1.37)	1.42 (1.42)
C5−C6	1.39 (1.39)	1.38 (1.39)	1.39 (1.39)	1.37 (1.36)
C6−C1	1.41 (1.39)	1.42 (1.40)	1.41 (1.44)	1.42 (1.41)
Fe−Cp[b]	1.74 (1.74)	1.78 (1.78)	1.74 (1.74)	1.78 (1.77)
Fe−P	2.26 (2.19)	2.29 (2.24)	2.27 (2.19)	2.30 (2.25)
	2.26 (2.18)	2.30 (2.26)	2.26 (2.18)	2.30 (2.24)
C4−X	1.38 (1.38)	1.35 (1.37)	1.41 (1.41)	1.36 (1.37)
δ[c]	87 (115)	96 (97)	89 (106)	90 (24)

[a] Refer to Chart 1 for labeling (experimental values are given in parentheses). [b] Cp = Cp centroid. [c] Dihedral angle Fe−Cp−C1−C6. [d] Experimental value given for a selected molecule in the asymmetric unit.[1e]

Calculations on the Fe(III) cationic species reveal that the HOMO of the neutral compound is formally depopulated upon oxidation. Atomic Hirshfeld charges for the neutral and cationic compounds are given in Table 6.

3. Energy Decomposition of the Fe−C Bond in Fe(II) Acetylides. The Fe−C bond dissociation energy was computed for **1a**-H−**1j**-H of C_s symmetry, considering an heterolytic process, i.e. the bonding energy (BDE) between $[(H_3P)_2(\eta^5\text{-}C_5H_5)Fe]^+$ and $[(C{\equiv}C)\text{-}1,4\text{-}(C_6H_4)X]^-$ fragments. The latter can be split according to the general *transition state* method of Ziegler and Rauk (eq

Table 4. Energy, Electron Occupancy, and FMO Decomposition of $(PH_3)_2(\eta^5\text{-}C_5H_5)Fe(C{\equiv}CC_6H_4X)$ Model Complexes (X = NO_2, CN, Br, H, OMe, NH_2)

	MO for **1a-H** (X = NO_2)								
	55a	54a	53a	52a	51a	50a	49a	48a	47a
e (eV)	−1.39	−1.27	−2.90	−3.03	−4.64	−4.83	−5.27	−6.04	−6.15
occ	0	0	0	0	2	2	2	2	2
% Fe	14	61	55	2	61	53	69	48	1
% Cp	23	21	23	0	8	3	8	20	0
% P	3	5	17	0	2	0	2	3	0
% C_a	1	3	0	7	6	8	4	18	1
% C_b	0	0	0	0	22	17	4	4	0
% C (Ph)	3	0	0	28	0	15	5	22	0
% NO_2	2	0	0	63	0	4	1	2	97
	MO for **1b**-H (X = CN)								
	51a	50a	49a	48a	47a	46a	45a	44a	43a
e (eV)	−1.31	−2.13	−2.19	−2.82	−4.55	−4.70	−5.17	−5.89	−6.34
occ	0	0	0	0	2	2	2	2	2
% Fe	0	18	44	56	61	51	68	50	25
% Cp	0	7	13	23	8	2	9	2	2
% P	0	11	4	16	2	0	2	0	1
% C_a	0	14	10	0	6	9	5	16	42
% C_b	0	0	0	0	22	17	3	2	27
% C (Ph)	100	47	16	0	0	16	5	22	0
% CN	0	13	5	0	0	3	1	5	0
	MO for **1d**-H (X = Br)								
	50a	49a	48a	47a	46a	45a	44a	43a	42a
e (eV)	−1.11	−1.36	−1.96	−2.61	−4.33	−4.40	−4.95	−5.57	−6.06
occ	0	0	0	0	2	2	2	2	2
% Fe	0	3	57	55	59	44	68	53	26
% Cp	0	1	19	23	8	2	9	1	2
% P	1	1	5	16	2	0	2	0	1
% C_a	0	15	9	0	6	12	5	7	41
% C_b	0	2	0	0	22	18	2	1	27
% C (Ph)	97	68	0	0	0	19	5	21	0
% Br	0	3	0	0	0	3	1	9	0
	MO for **1f**-H (X = H)								
	47a	46a	45a	44a	43a	42a	41a	40a	39a
e (eV)	−0.95	−1.10	−1.83	−2.48	−4.18	−4.24	−4.80	−5.46	−5.88
occ	0	0	0	0	2	2	2	2	2
% Fe	13	7	56	55	59	45	67	56	0
% Cp	1	2	18	23	8	2	9	2	0
% P	19	7	6	17	2	0	2	0	0
% C_a	5	11	9	0	7	12	5	14	0
% C_b	0	1	0	0	23	19	2	2	0
% C (Ph)	27	50	0	0	0	20	6	22	100
% H	0	0	0	0	0	0	0	0	0
	MO for **1i**-H (X = OMe)								
	53a	52a	51a	50a	49a	48a	47a	46a	45a
e (eV)	−0.82	−0.95	−1.74	−2.41	−4.04	−4.13	−4.66	−5.21	−5.83
occ	0	0	0	0	2	2	2	2	2
% Fe	2	16	56	57	35	57	64	57	24
% Cp	0	0	16	21	0	5	6	0	0
% P	3	27	9	18	0	0	1	0	0
% C_a	7	2	8	0	13	6	4	5	38
% C_b	0	0	0	0	16	21	0	0	24
% C (Ph)	85	11	0	0	23	0	4	20	0
% OMe	1	0	0	0	4	0	2	7	0
	MO for **1j**-H (X = NH_2)								
	50a	49a	48a	47a	46a	45a	44a	43a	42a
e (eV)	−0.72	−0.91	−1.70	−2.36	−3.91	−4.08	−4.59	−5.07	−5.77
occ	0	0	0	0	2	2	2	2	2
% Fe	0	17	56	54	30	59	65	62	27
% Cp	0	3	18	23	1	7	10	0	2
% P	0	20	7	17	0	2	3	0	1
% C_a	0	1	9	0	16	7	4	1	40
% C_b	0	0	0	0	15	23	0	2	25
% C (Ph)	99	6	0	0	28	0	7	18	0
% NH_2	0	0	0	0	9	0	3	11	0

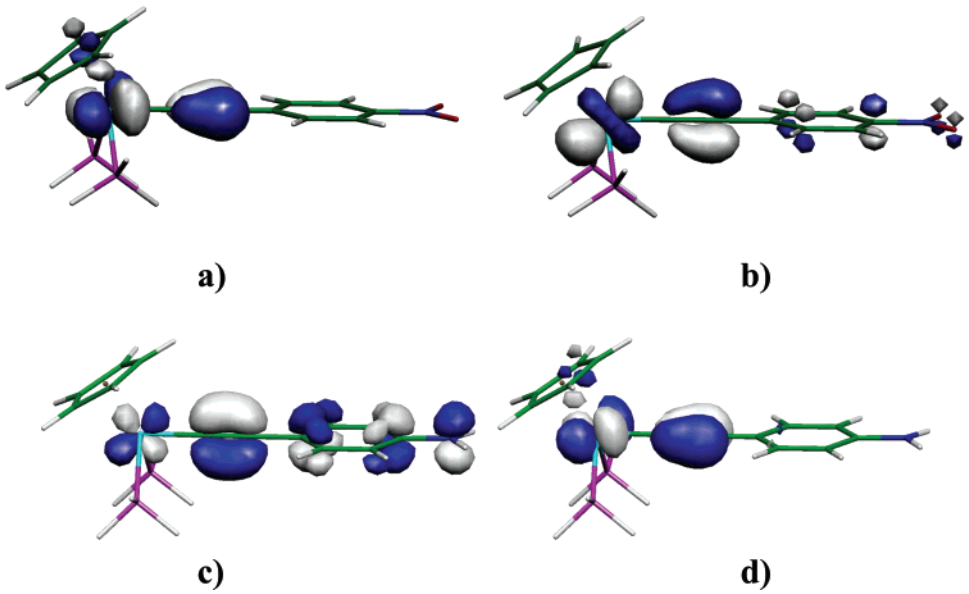

Figure 7. Plot of the HOMO (left) and HOMO-1 (right) of $(H_3P)_2(\eta^5\text{-}C_5H_5)Fe(C{\equiv}C)\text{-}1,4\text{-}(C_6H_4)X$ complexes: (a, b) X = NO_2; (c, d) X = NH_2. The contour value is 0.05 [e/bohr^3]$^{1/2}$.

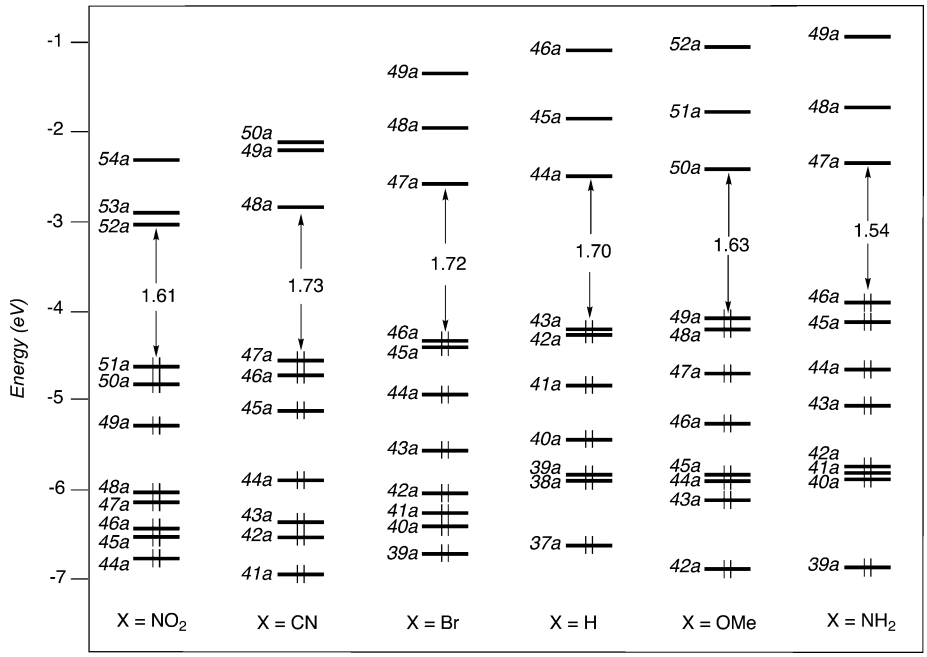

Figure 8. Energy (eV) of the frontier orbitals of the complexes $(H_3P)_2(\eta^5\text{-}C_5H_5)Fe(C{\equiv}C)\text{-}1,4\text{-}(C_6H_4)X$ (**1a**-H−**1j**-H; X = NO_2, CN, Br, H, OMe, NH_2).

Table 5. HOMO−LUMO Gaps (Δ*E*) for $[(PH_3)_2(\eta^5\text{-}C_5H_5)Fe(C{\equiv}CC_6H_4X)]_n^+(PF_6^-)_n$ Model Complexes (n = 0, 1; X = NO_2, CN, Br, H, OMe, NH_2) and Ionization Potentials for Fe(II) Parents (*n* = 0)

	1a-H	**1b**-H	**1d**-H	**1f**-H	**1i**-H	**1j**-H
X	NO_2	CN	Br	H	OMe	NH_2
Δ*E*	1.610	1.733	1.723	1.700	1.632	1.543
IP[a]	6.665	6.571	6.301	6.222	5.941	5.817
ΔIP[b]	0.140	0.140	0.143	0.101	0.161	0.209

[a] Vertical IPs. [b] ΔIP = IP(vertical) − IP(adiabatic).

1) into separate terms (see the Experimental Section for computational details).[30,31]

$$\mathrm{BDE}(\Delta H) = \Delta E_{\mathrm{el}} + \Delta E_{\mathrm{orb}} + \Delta E_{\mathrm{Pauli}} \qquad (1)$$

ΔE_{orb} itself can further be decomposed into contributions representing the σ donation ($\Delta E\sigma$), the metal-to-ligand back-donation ($\Delta E\pi_{M\to L}$), and the ligand-to-metal forward-donation ($\Delta E\pi_{L\to M}$) terms (Table 7).

The Pauli term in the Fe−C bond is mostly due to a repulsive interaction between the filled π orbitals of the acetylide and the filled π-type orbitals (with strong d character) of the metallic fragment. This term decreases throughout the series, corresponding to an increasing repulsive interaction. Its variations dominate those corresponding to the $\Delta E\pi_{M\to L}$ and $\Delta E\pi_{L\to M}$ terms (i.e. bonding contributions to the BDE). The latter are identified as back-bonding ($\Delta E\pi_{M\to L}$ terms), which corresponds to a net electron transfer from occupied metallic orbitals toward the empty π* orbitals of the

(30) Ziegler, T.; Rauk, A. *Inorg. Chem.* **1979**, *18*, 1558−1565.
(31) Bickelhaupt, F. M.; Baerends, E. J. *Rev. Comput. Chem.* **2000**, *15*, 1−86.

Table 6. Calculated Hirshfeld Charges for $[(PH_3)_2(\eta^5\text{-}C_5H_5)Fe(C{\equiv}CC_6H_4X)]_n^+(PF_6^-)_n$ Complexes (n = 0, 1; X = NO_2, CN, Br, H, OMe, NH_2)

	1a-H	**1a**-H$^+$	**1b**-H	**1b**-H$^+$	**1d**-H	**1d**-H$^+$	**1f**-H	**1f**-H$^+$	**1i**-H	**1i**-H$^+$	**1j**-H	**1j**-H$^+$
X	NO_2	NO_2	CN	CN	Br	Br	H	H	OMe	OMe	NH_2	NH_2
Fe	−0.073	+0.009	−0.074	+0.001	−0.076	−0.014	−0.076	−0.011	−0.078	−0.025	−0.078	−0.032
C_a	−0.157	−0.140	−0.162	−0.136	−0.170	−0.130	−0.174	−0.133	−0.178	−0.128	−0.179	−0.128
C_b	−0.110	−0.011	−0.114	−0.020	−0.118	−0.036	−0.114	−0.026	−0.118	−0.050	−0.118	−0.058
C1	+0.014	+0.013	+0.010	+0.015	+0.003	+0.014	−0.001	+0.011	−0.013	+0.009	−0.016	+0.008
C2	−0.048	−0.033	−0.051	−0.030	−0.051	−0.024	−0.059	−0.031	−0.058	−0.025	−0.058	−0.026
C3	−0.046	−0.029	−0.041	−0.020	−0.066	−0.041	−0.060	−0.032	−0.080	−0.053	−0.079	−0.049
C4	+0.019	+0.040	−0.005	+0.028	−0.010	0.023	−0.066	−0.016	+0.060	0.105	+0.033	+0.080
C5	−0.046	−0.029	−0.041	−0.021	−0.066	−0.041	−0.060	−0.031	−0.074	−0.045	−0.079	−0.049
C6	−0.048	−0.033	−0.051	−0.032	−0.051	−0.025	−0.059	−0.031	−0.056	−0.028	−0.058	−0.025
X	+0.190	+0.206	+0.060	+0.076	−0.047	+0.066	+0.045	+0.070	−0.117	−0.070	−0.205	−0.125

Table 7. Heterolytic Bond Energies (BDEs) and Bond Energy Decomposition of the Fe−C Bond in $(PH_3)_2(\eta^5\text{-}C_5H_5)Fe{-}C{\equiv}CC_6H_4X$ Complexes (X = NO_2, CN, Br, H, OMe, NH_2)

	1a-H	**1b**-H	**1d**-H	**1f**-H	**1i**-H[a]	**1j**-H
X	NO_2	CN	Br	H	OMe	NH_2
ΔE_{Pauli}	−7.37	−7.37	−7.58	−7.61	−7.36	−8.10
ΔE_{orb}[b]	+3.82	+3.97	+3.85	+3.79	+3.91	+4.23
$\Delta E\sigma$	*+1.74*	*+1.95*	*+1.86*	*+1.85*	*+1.90*	*+2.15*
$\Delta E\pi_{M\to L}$	*+1.68*	*+1.59*	*+1.52*	*+1.44*	*+1.48*	*+1.52*
$\Delta E\pi_{L\to M}$	*+0.40*	*+0.43*	*+0.47*	*+0.50*	*+0.53*	*+0.56*
ΔE_{el}	+10.20	+10.19	+10.47	+10.69	+10.56	+11.06
BDE(ΔH)	+6.66	+6.77	+6.72	+6.87	+7.13	+7.16

[a] Obtained for the less stable conformation with the OMe substituent perpendicular to the phenyl ring. [b] $\Delta E_{orb} = \Delta E\sigma + \Delta E\pi_{M\to L} + \Delta E\pi_{L\to M}$ (i.e. the sum of the three values given in italics).

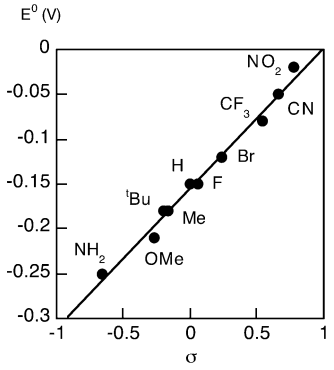

Figure 9. Plot of the Fe(III)/Fe(II) oxidation potentials (V) of the complexes $[(\eta^2\text{-dppe})(\eta^5\text{-}C_5Me_5)Fe(C{\equiv}C)\text{-}1,4\text{-}(C_6H_4)X]^+(PF_6)^-$ (X = NO_2, CN, CF_3, F, Br, H, Me, ^{t}Bu, OMe, NH_2) vs Hammett ESPs (σ) in CH_2Cl_2.

alkynyl ligand, and forward-bonding ($\Delta E\pi_{L\to M}$ terms), which corresponds to the transfer of electronic density from the filled π MO of the acetylide fragment to empty MOs of the metallic fragment. For compounds with substituents presenting ESPs with relatively "moderate" values (**1d**-H−**1i**-H), the variations of $\Delta E\pi_{M\to L}$ and $\Delta E\pi_{L\to M}$ terms partly cancel each other. This indicates an overall constancy of the *bonding* π interactions in these complexes. Similar trends are observed in both the perpendicular and parallel π manifold relative to the phenyl plane, but as expected, the changes are less pronounced in the π manifold which is not conjugated with the substituent (see the Experimental Section).

Hammett Linear Free Energy Relationships for Fe(II) Acetylides. Although the Hammett methodology is often criticized because of its essentially empirical foundation, it constitutes an interesting way to investigate more specifically the influence of the X substituent on various electronic properties of the $[(\eta^2\text{-dppe})(\eta^5\text{-}C_5Me_5)Fe(C{\equiv}CC_6H_4X)]^{n+}(PF_6^-)_n$ complexes (n = 0, 1; X = NO_2, CN, CF_3, Br, F, H, Me, ^{t}Bu, OMe, NH_2).[1b] Thus, in conjunction with the DFT computations presently made for the model complexes $[(PH_3)_2(\eta^5\text{-}C_5H_5)Fe(C{\equiv}CC_6H_4X)]^{n+}(PF_6^-)_n$ (n = 0, 1; X = NO_2, CN, Br, H, OMe, NH_2), we have looked for linear free energy relationships (LFERs) with electronic substituent parameters (ESPs), involving characteristic redox and spectroscopic data of the experimentally isolated complexes.

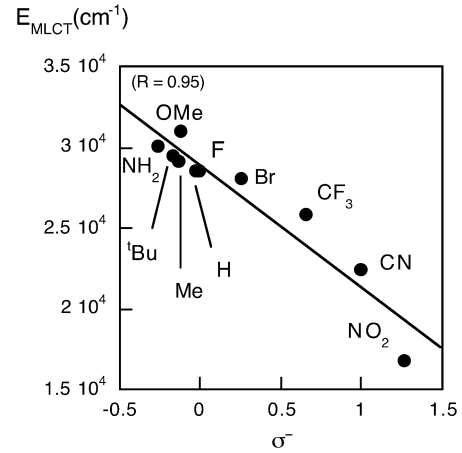

Figure 10. a. Plot of the MLCT energy (cm^{-1}) vs σ^- ESPs for $(\eta^2\text{-dppe})(\eta^5\text{-}C_5Me_5)Fe(C{\equiv}C)\text{-}1,4\text{-}(C_6H_4)X$ complexes (X = NO_2, CN, CF_3, F, Br, H, Me, ^{t}Bu, OMe, NH_2).

A very good linear correlation (R = 0.99; eq 2) is obtained between the σ Hammett ESPs[32] and the redox potentials corresponding to the iron-centered Fe(III)/Fe(II) oxidation of **1a**−**j** (Figure 9). The weak solvent dependence of the slope confirms the dominant intramolecular nature of the electronic effect. The positive slope reflects the fact that an electron-releasing substituent renders the iron-centered oxidation more facile, whereas an electron-withdrawing one has the reverse effect and shifts it anodically.

$$E_0\,(\mathrm{V}) = 0.157\sigma - 0.154 \qquad (2)$$

Correlation of the energy (in cm^{-1}) of the lowest lying electronic (MLCT) transition in **1a**−**j** with σ gives a poor linear fit (R = 0.88). However, a much better fit is obtained when the σ^- ESPs are used in place of σ (R = 0.95; Figure 10 and eq 3).[32] The negative slope reflects the bathochromic shift exerted by electron-withdrawing substituents, while the use of σ^- reveals

(32) Hansch, C.; Leo, A.; Taft, R. W. *Chem. Rev.* **1991**, *91*, 165−195.

$$E_{MLCT}\,(cm^{-1}) = -7622\,\sigma^- + 28\,876 \qquad (3)$$

the dominance of mesomeric interactions in this substituent effect.

Finally, a very good correlation is obtained as well with the ^{13}C NMR shifts of the α-carbon of the acetylide ligand (Figure 11) using σ^- (eq 4a; $R = 0.99$). This clearly indicates that the strongest electron-withdrawing substituents induce a marked deshielding of the corresponding ^{13}C NMR shift. In contrast, a very poor correlation is stated for the ^{13}C NMR shift of the β-carbon atom with σ^- ESPs (eq 4b; $R = 0.78$).

$$\delta C_\alpha\,(ppm) = 20.20\sigma^- + 136.6 \qquad (4a)$$

$$\delta C_\beta\,(ppm) = 2.3\sigma^- + 119.8 \qquad (4b)$$

Discussion

Electronic Structures of Electron-Rich Fe(II) and Fe(III) Model Complexes. DFT calculations indicate overall an energetic ordering and spatial distribution of the frontier MO's similar to that previously found for piano-stool Fe(II) acetylide complexes containing electron-poorer metal fragments, such as $(CO)_2(\eta^5\text{-}C_5H_5)Fe{-}C{\equiv}CPh$ (**2**) for instance.[16−18] In accordance

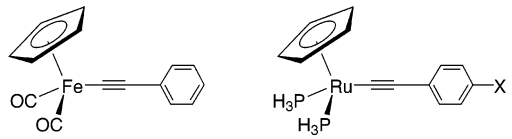

2 **3a-3c**

with the more electron-rich nature of the metal center in complexes **1a**-H−**1j**-H, the occupied frontier orbitals are slightly higher in energy than in **2**.[16,19,20b] Due to the σ-polarization of the M−C bond with electron-rich metal centers, the α-acetylide carbon atom is more negatively charged in these complexes than in **2**. A similar feature was also recently noticed by Low and co-workers from DFT calculations carried out on the related model complexes **3a**−**3c**.[20b] Similarly to **2** and despite the more electron-releasing nature of the "$(Ph_3P)_2(\eta^5\text{-}C_5H_5)Fe$" fragment relative to "$(CO)_2(\eta^5\text{-}C_5H_5)Fe$", the largest ligand-based contribution to the HOMO comes from the β-carbon atom of the Fe−C≡C fragment along the whole series from **1a**-H to **1j**-H (Table 4), regardless of the nature of the X substituent.[18a]

Upon oxidation, the negative charge on the Fe−C≡C fragment decreases, the largest change taking place at the metal center.[33] The metal atom itself bears some positive charge only with the most electron-withdrawing substituents (X = NO_2, CN, Br). The acetylide ligand still carries a negative charge, with most of it located at C_α. The electronic structures of the Fe−C≡C fragment in Fe(III) model complexes **1a**-H^+−**1j**-H^+ resemble those of their Fe(II) parents, a slight shortening being computed for the Fe−C bond upon oxidation. This can

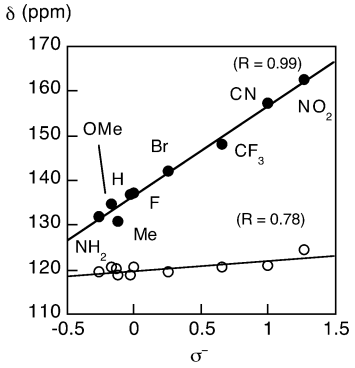

Figure 11. Plot of the alkynyl ^{13}C NMR shifts (ppm) of C_α (●) and C_β (○) vs σ^- ESPs for $(\eta^2\text{-dppe})(\eta^5\text{-}C_5Me_5)Fe(C{\equiv}C)\text{-}1,4\text{-}(C_6H_4)X$ complexes (X = NO_2, CN, CF_3, F, Br, H, Me, ^{t}Bu, OMe, NH_2).

easily be understood by considering the counteracting structural influences operating at this fragment upon oxidation. Indeed, oxidation (i) diminishes the metal-to-acetylide back-donation due to contraction of the metal orbitals but oppositely (ii) promotes M−C bonding by transforming a repulsive four-electron−two-orbital π-type interaction into a more favorable three-electron−two-orbital one. This results in the strengthening of the σ-type interaction between the metal and the acetylide fragment.[17a,19a] As a result, neither the Fe−C nor the C≡C bond lengths constitute truly reliable tags for probing the oxidation state of the metal center, as already stated for $(\eta^2\text{-dppe})(C_5Me_5)Fe$ fragments in polynuclear analogues.[15b,c] This statement is confirmed by the X-ray data (see below).[1a,e]

Substituent Effect on the Strength of the Fe−C Bond in Fe(II) Model Complexes. The heterolytic Fe−C bond energies (BDE) were derived for Fe(II) model complexes with imposed C_s symmetry (Table 7). The data show an overall increase of 7% in the total Fe−C BDE on going from the nitro to the amino substituent, relative to the mean value for the series (6.88 eV/158.6 kcal). This is a relatively important effect (ca. 11 kcal) for a substituent positioned six bonds apart, which reveals the capability of the phenylalkynyl spacer to efficiently convey electronic interactions. This significant increase actually results from interplay of conflicting influences, as revealed by the decomposition of the bond energy made, as shown hereafter (eq 1).[34]

The present computations indicate that, for all complexes, net back-bonding ($\Delta E\pi_{M\to L}$) largely overcomes net forward-bonding ($\Delta E\pi_{L\to M}$). For electron-poorer acetylides such as **2**, Lichtenberger and others have shown that the repulsive d−π interaction dominates over π interactions and that back-donation is at best very small.[16,17a,c,18a] Back-donation is still weak for the compounds **1a**−**j** but appears to be relatively more important than in **2**. Indeed, it represents a sizable contribution to the bond energy, especially for the compounds bearing the most electron-withdrawing substituents such as **1a**-H and **1b**-H, where it amounts to more than 15% of the total heterolytic BDE (Table 7).

As shown in Figure 12a, when the data are plotted with respect to σ ESPs, back-donation, represented by $\Delta E\pi_{M\to L}$, first decreases along the series from **1a**-H to

(33) For all Fe(III) model complexes **1a**-H^+−**1j**-H^+, calculations indicate that the electronic hole is mostly located on the metal fragment. In the corresponding Ru complex **3a**, approximately half of the positive charge originates from the metal center and half from the alkynyl ligand.[20b]

(34) Ziegler, T. *Metal−Ligand Interactions: From Atoms, to Clusters, to Surfaces*; Kluwer: Dordrecht, The Netherlands, 1992.

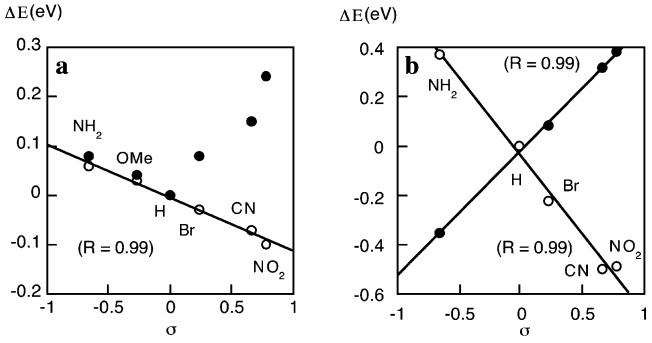

Figure 12. Plots of relative energies (eV) for various contributions to the heterolytic BDE computed for $(PH_3)_2(\eta^5\text{-}C_5H_5)Fe(C{\equiv}C)\text{-}1,4\text{-}(C_6H_4)X$ complexes (X = NO_2, CN, Br, H, OMe, NH_2) vs Hammett ESPs (σ): (a) $(\Delta E\pi_{M\rightarrow L})_x - (\Delta E\pi_{M\rightarrow L})_H$ (●) and $(\Delta E\pi_{L\rightarrow M})_x - (\Delta E\pi_{L\rightarrow M})_H$ (○); (b) $(\Delta E_{Pauli} + \Delta E\pi_{M\rightarrow L} + \Delta E\pi_{L\rightarrow M})_x - (\Delta E_{Pauli} + \Delta E\pi_{M\rightarrow L} + \Delta E\pi_{L\rightarrow M})_H$ (●) and $(\Delta E_{elec})_x - (\Delta E_{elec})_H$ (○).

1f-H and then increases slightly again for **1i**-H and **1j**-H, which bear the less electron-withdrawing substituents. In contrast, forward-donation increases steadily from **1a**-H to **1j**-H, giving a very good linear correlation with Hammett ESPs (R = 0.99). With these ESPs, a comparable linear correlation (Figure 12b) is observed with the $\Delta E_{Pauli} + \Delta E\pi_{M\rightarrow L} + \Delta E\pi_{L\rightarrow M}$ sum (R = 0.99).[35] This sum, which increases for electron-withdrawing X substituents, can be viewed as representing roughly the relative stabilization originating from π electronic overlap along the Fe−C bond. Consequently, the important decrease of the Fe−C π bond order stated for electron-releasing substituents mainly results not only from an enhancement of the repulsive four-electron−two-orbital d−π interactions between the Fe(II) center and the α-acetylide carbon atom but also, to a smaller extent, from the concomitant decrease of the stabilizing metal-to-ligand back-bonding π interactions. Finally, a good linear correlation (R = 0.99) is also obtained with the ΔE_{elect} term (Figure 12b).[35] In contrast with the previous π contribution, this contribution becomes more and more stabilizing as the electron-releasing capability of the X substituent increases. This reflects the increasing electrostatic stabilization of the Fe−C bonding, which is also concomitant with a decrease of its local polarization (Table 6). This contribution is mostly responsible for the computed increase in heterolytic BDE from **1a**-H to **1j**-H.

Computed vs Experimental Data for Fe(II) and Fe(III) Acetylides. Comparison between theoretical data computed for **1a**-H/**1a**-$H^+PF_6^-$ through **1j**-H/**1j**-H^+-PF_6^- and the experimental data gathered for **1a**/**1a**$^+$-PF_6^- through **1j**/**1j**$^+PF_6^-$ provides a simple way to validate the predictive values of computationally simpler model complexes for discussing the electronic properties of the latter.

1. Bond Lengths. For all the Fe(II) and Fe(III) acetylides, DFT-computed Fe−$Cp_{centroid}$ and Fe−P bond distances (Table 3) are systematically a few hundredths of an angstrom longer than the corresponding X-ray values (ca. 0.05 and 0.07 Å, respectively). Similarly, the computed Fe−C_α bond lengths are respectively slightly longer and shorter (0.01−0.05 Å) in the Fe(II) and Fe(III) model complexes than in the solid-state structures. To some extent, this can be ascribed to the use of C_5H_5 and PH_3 ligands in place of C_5Me_5 and dppe, respectively.[22d,36] The computed Fe−C_α bond lengths appear to be hardly affected by the nature of the X substituent. They slightly lengthen in Fe(II) model complexes from 1.89 Å for **1a**-H (X = NO_2) to 1.91 Å for **1j**-H (X = NH_2) and conversely shorten in Fe(III) complexes from 1.85 Å for **1a**-H^+ (X = NO_2) to 1.84 Å for **1j**-H^+ (X = NH_2). Such a trend is also apparent in the X-ray data for **1a**/**1a**$^+PF_6^-$ through **1j**/**1j**$^+PF_6^-$.[1a,e] Calculations suggest an overall quinone-like deformation of the functional aryl group of the 1,4-arylethynyl ligand in Fe(II) acetylides. Experimentally, this is hardly detectable, given the esds.[1a] In fact, after oxidation of the metal center, the bond distances within the phenylethynyl core are not significantly altered, according to the X-ray data. The largest change takes place in the metal atom coordination sphere and around the X substituent. Thus, a slight expansion of the coordination sphere is observed, which results from the decreased back-donation toward the cyclopentadienyl and phosphorus FMOs.[37] Actually, a lengthening of the Fe−$Cp^*_{centroid}$ and Fe−P distances of 0.02−0.05 and 0.02−0.07 Å, respectively, is stated for all compounds upon oxidation. Conversely, an overall shortening (ca. 0.01 Å) takes place for the Fe−C_α bond. However, in agreement with the DFT data, the contraction is slightly overestimated by the computations (0.04−0.06 Å). Interestingly, all conformations found after geometry optimization show a dihedral angle among the Fe atom, the Cp centroid, and the phenyl ring of close to 90°, which roughly corresponds to the conformations observed in the solid state. In conclusion, the agreement between theoretical and experimental values is quite satisfactory. With a maximum deviation of 0.05 Å, the few discrepancies existing with the experimental bond distances remain within experimental error. The weak structural differences between the Fe(II) and Fe(III) parents suggest already that λ_{in}, the internal contribution of the reorganization energy ($\lambda = \lambda_{in} + \lambda_{out}$) associated with the oxidation of the Fe(II) center, will be weak (see below).[38]

2. Ionization Potentials. Gas-phase vertical ionization potentials (IPs) were computed for the Fe(II) acetylide complexes (Table 5). These data can be compared to the corresponding redox potential values derived from cyclic voltammetry (CV) experiments. Indeed, for redox species with similar diffusion rates at the electrode, a simple relationship between gas-phase IPs and redox potentials can be derived from thermochemical cycles (eq 5).[39] In eq 5, the $\Delta(\Delta F°)_{solv}$ term

$$E° \text{ (V)} = (\text{IP})_{gas} + \Delta(\Delta F°)_{solv} + C_{solv} \qquad (5)$$

(=$\Delta F°[\text{Fe(II)}]_{solv} - \Delta F°[\text{Fe(III)}]_{solv}$) mainly corresponds to the change in free energy of solvation between the two redox species involved in the process and is mostly

(35) The data for the methoxy compound **1i**-H have been omitted, since these values do not correspond to the most stable conformation.

(36) Costuas, K.; Saillard, J.-Y. *Organometallics* **1999**, *18*, 2505−2512.
(37) Orpen, A. G.; Connelly, N. G. *Organometallics* **1990**, *9*, 1206−1210.
(38) Astruc, D. *Electron Transfer and Radical Processes in Transition-Metal Chemistry*; VCH: New York, 1995.
(39) Streitweiser, A., Jr. *Molecular Orbital Theory for Organic Chemists*; Wiley: London, 1961.

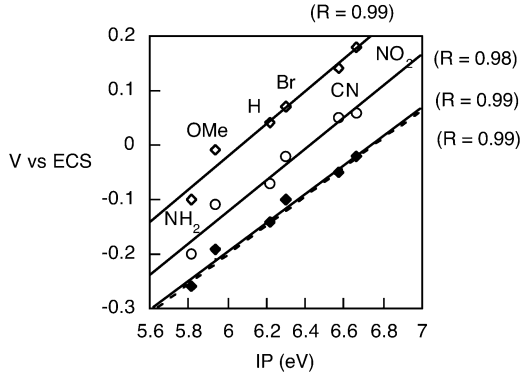

Figure 13. Plot of the redox Fe(II)/Fe(III) oxidation potentials (V) vs computed vertical ionization potentials (eV) for (η^2-dppe)(η^5-C_5Me_5)Fe(C≡C)-1,4-(C_6H_4)X complexes (X = NO_2, CN, Br, H, OMe, NH_2) in THF (○), acetone (◇), CH_3CN (◆), and CH_2Cl_2 (dotted line).

determined by the solvent used. In addition, this term also incorporates solvent-dependent entropic contributions and terms associated with the relaxation of the oxidized species at the electrode surface.[40] Finally, the additional term C_{solv} includes the contribution of the free energy change of the electron at the electrode, $[(\Delta F°)_e]_{electr}/F$, which should be constant for a given solvent/electrode system.[39] Thus, when the $\Delta(\Delta F°)_{solv}$ term is constant, a linear relationship with a slope of unity results between experimental redox potentials and gas-phase vertical IPs.

A linear relation is presently found between the DFT-computed vertical IPs of **1a**-H−**1i**-H and the Fe(III)/Fe(II) redox potentials of the corresponding **1a**−**i** acetylides in various solvents of differing polarity. Good linear correlations with comparable slopes are obtained (Figure 13). The nature of the solvent hardly modifies the slopes of the regression lines (0.26−0.30) but shifts the potentials by a constant value. This solvent-induced shift in the values of the Fe(III)/Fe(II) redox potentials is quite important for a given compound and can exceed the range spanned by all substituents in a given solvent (ca. 0.26 V in CH_2Cl_2). However, in contrast with what had been previously stated with the closely related complexes (η^2-dppe)(η^5-C_5Me_5)FeX complexes recently reported by Tilset and co-workers (X = F, Cl, Br, Me, H, I; **5a**−**f**),[41] the observed slopes differ from unity and are much closer to 0.30, which represents a severe dampening of the IP influence. This suggests that, at least in part, the $\Delta(\Delta F°)_{solv}$ term in eq 5 is presently not constant across the **1a**−**j** series, but more and more negative in proportion to the increasing IPs, to account for the *linear* fits obtained. After having verified that the vertical IPs used in the correlations did scale linearly with the Hammett ESPs (see the Supporting Information), we think that the nonunity slopes reveal the determining role of the X substituent in the solvation effects ($\Delta(\Delta F°)_{solv}$) during the oxidation process at the electrode.

Thus, while clearly confirming the expected linear dependence of the vertical IPs with the X substituent, the present correlations also suggest a dependence of (part of) the differential solvation term $\Delta(\Delta F°)_{solv}$ in eq 5 on the substituent. That particular substituent effect along the **1a**-H−**1i**-H series is much larger in magnitude than the related change between the computed gas-phase relaxation energies (ΔIP in Table 5). In relation to Marcus theory,[38] ΔIP can be envisioned as an approximation of the internal contribution (λ_{in}) to the reorganization energy λ. When λ is approximated as $\Delta(\Delta F°)_{solv}$, these data confirm that λ_{in} must be quite weak and roughly constant in comparison to λ (i.e. $\lambda_{out} \gg \lambda_{in}$). This means in turn that the outer contribution (λ_{out}) to the reorganization energy during oxidation of (η^5-dppe)(η^5-C_5Me_5)Fe−C≡C-1,4-(C_6H_4)X complexes is more sensitive to the nature of the X substituent than the internal contribution (λ_{in}).

Table 8. Computed $\nu_{C\equiv C}$ (cm^{-1}) Values for (PH_3)$_2$(η^5-C_5H_5)Fe(C≡CC_6H_4X) Model Complexes vs Experimental Values for the Corresponding (η^2-dppe)(η^5-C_5Me_5)Fe(C≡CC_6H_4X) Complexes (X = NO_2, CN, Br, H, OMe, NH_2)

	1a-H	**1b**-H	**1d**-H	**1f**-H	**1i**-H	**1j**-H
X	NO_2	CN	Br	H	OMe	NH_2
$\nu_{C\equiv C}$						
computed	2036	2044	2050	2051	2050	2059
exptl[a]	2036 (vs) 2008 (s)	2050 (vs) 2025 (vs)	2054	2053	2058	2060

[a] Recorded in CH_2Cl_2 at 25 °C.[1a,b]

3. Spectroscopic Data. Some characteristic infrared and UV−vis spectroscopic transitions were computed for the model complexes **1a**-H−**1j**-H and compared to the corresponding experimental data available for **1a**−**j**.[1a,b] The calculated and experimental C≡C stretching frequencies are summarized in Table 8. Most of the computed values agree with the experimental ones within 10 cm^{-1}. For **1a**-H and **1b**-H, calculations do not reproduce the Fermi coupling observed for **1a**,**b**.[1b] The computed values certainly correspond to the *Fermi-decoupled* $\nu_{C\equiv C}$ fundamental stretching modes, since the corresponding wavenumbers are bracketed by the two absorptions experimentally found. In addition, calculations indicate a slight coupling between the triple-bond stretching mode and the ≡C−C_{aryl} stretching for all model complexes investigated. A combination mode or a harmonic mode involving the latter stretch is likely at the origin of the Fermi coupling observed for **1a**−**c**.[1b]

The TD-DFT calculated lowest excitation energies of selected allowed transitions for **1a**-H−**1j**-H are listed in Table 9. These are tabulated together with experimental absorption peak maxima.[1a] Only a few transitions below 4.0 eV have a significant oscillator strength (*f*) and might be experimentally observed. None of these correspond to a simple electronic transition between two MOs. Indeed, calculations indicate that there is a considerable orbital mixing/configuration interaction for the most important transitions, involving more than two MOs (Figure 5). The maximum of the low-energy absorption band reported for **1a**−**j** agrees roughly with the most intense transitions computed for the model complexes **1a**-H−**1j**-H within 0.4 eV (ca. 3200 cm^{-1}). In the 900−300 nm spectral range (ca. 1.4−4.0 eV), several peaks are observed only in the case of **1a** (X = NO_2) and **1d** (X = Br). However, the non-Gaussian shape of

(40) Li, J.; Fisher, C. L.; Chen, J. L.; Bashford, D.; Noodleman, L. *Inorg. Chem.* **1996**, *35*, 4694−4702.
(41) Tilset, M.; Fjeldahl, I.; Hamon, J.-R.; Hamon, P.; Toupet, L.; Saillard, J.-Y.; Costuas, K.; Haynes, A. *J. Am. Chem. Soc.* **2001**, *123*, 9984−10000.

Table 9. Energy (eV) and Composition of the First UV−Vis Electronic Transitions for $(PH_3)_2(\eta^5\text{-}C_5H_5)Fe(C{\equiv}CC_6H_4X)$ Model Complexes vs Experimental Values (eV) for Corresponding the $(\eta^2\text{-dppe})(\eta^5\text{-}C_5Me_5)Fe(C{\equiv}CC_6H_4X)$ Complexes (X = NO_2, CN, Br, H, OMe, NH_2)

compd (X)	calcd[a] ν_{max} (f[b])	composition	major assignt	obsd[a] ν_{max} (ϵ[c])
1a-H	2.10	61% 50a → 52a	Fe → $C_6H_4NO_2$	2.084
(NO_2)	(0.10)	30% 49a → 52a	Fe → $C_6H_4NO_2$	(13.0)
	2.43	62% 49a → 52a	Fe → $C_6H_4NO_2$	
	(0.22)	28% 50a → 52a	Fe → $C_6H_4NO_2$	
	3.31	67% 48a → 52a	Fe → $C_6H_4NO_2$	3.712
	(0.17)	17% 49a → 54a	Fe → Cp	(11.6)
		4% 50a → 52a		
1b-H	2.70	69% 46a → 49a	Fe → $C_2-C_6H_4CN$/Cp	2.786
(CN)	(0.09)	28% 45a → 49a	Fe → $C_2-C_6H_4CN$/Cp	(16.4)
	3.09	66% 45a → 49a	Fe → $C_2-C_6H_4CN$/Cp	3.203
	(0.28)	23% 46a → 49a	Fe → Cp	(10.3, sh)
1d-H	3.27	59% 45a → 51a	Fe → $C_2-C_6H_4Br$	3.204
(Br)	(0.05)	35% 45a → 49a	Fe → $C_2-C_6H_4Br$	(11.2, sh)
	3.45	32% 45a → 49a	Fe → $C_2-C_6H_4Br$	3.482
	(0.12)	32% 45a → 51a	Fe → $C_2-C_6H_4Br$	(13.8)
		26% 44a → 49a	Fe → $C_2-C_6H_4Br$	
	3.72	40% 45a → 53a		
	(0.09)	38% 44a → 49a		
		7% 43a → 48a		
		7% 45a → 49a		
	3.83	34% 43a → 48a	$C_2-C_6H_4Br$ → Cp	3.838
	(0.14)	16% 44a → 49a	Fe → $C_2-C_6H_4Br$	(16.4)
		12% 45a → 53a		
		10% 44a → 51a		
		9% 45a → 49a		
		6% 44a → 48a		
		4% 43a → 49a		
1f-H	3.53	52% 38a → 44a	C_2 → Fe−Cp	
(H)	(0.06)	14% 42a → 46a		
		12% 42a → 47a		
		5% 41a → 45a		
		5% 41a → 47a		
		5% 41a → 46a		
	3.57	27% 42a → 47a	Fe → Ph/PH_3	3.542
	(0.06)	23% 38a → 44a	C_2 → Fe−Cp	(13.6)
		23% 41a → 46a	Fe → Ph	
		13% 42a → 46a		
		8% 40a → 45a		
	3.94	35% 41a → 46a	Fe → Ph	
	(0.18)	14% 41a → 47a	Fe → Ph/PH_3	
		11% 40a → 45a		
		11% 42a → 46a		
		10% 42a → 47a		
		5% 40a → 46a		
		3% 42a → 49a		
1i-H	3.68	31% 49a → 54a	Fe → C_2−Ph	3.723
(OMe)	(0.11)	12% 47a → 52a	Fe → PH_3	(13.2)
		11% 46a → 51a		
		11% 47a → 54a		
		9% 49a → 53a		
1j-H	3.75	46% 44a → 49a	Fe → PH_3	3.856
(NH_2)	(0.13)	31% 46a → 51a	Fe → $C_2-C_6H_4NH_2$	(17.6)
		6% 44a → 51a		
		5% 46a → 55a		

[a] In eV (the calculated excited states are ^{1}A). [b] Computed transition moment. [c] Experimental absorption coefficients (ϵ) in 10^3 M^{-1} cm^{-1}.

the low-energy peak of most complexes also suggests the existence of several overlapping electronic transitions. Vibrational progressions would not satisfactorily rationalize these features, especially since in some cases the spectral envelope of this absorption appears to be solvent-dependent, as shown for **1b** in Figure 14. More importantly, the TD-DFT computations confirm that the low-energy absorption (2.084−3.856 eV) in **1a**−**j** corresponds to a metal-to-ligand charge transfer (MLCT). This is in agreement with the experimental (and computed) hypsochromic shift of this band when X becomes more and more electron-releasing.[1a] Analogous results based on DFT calculations were recently reported with related transition-metal acetylides.[28,42]

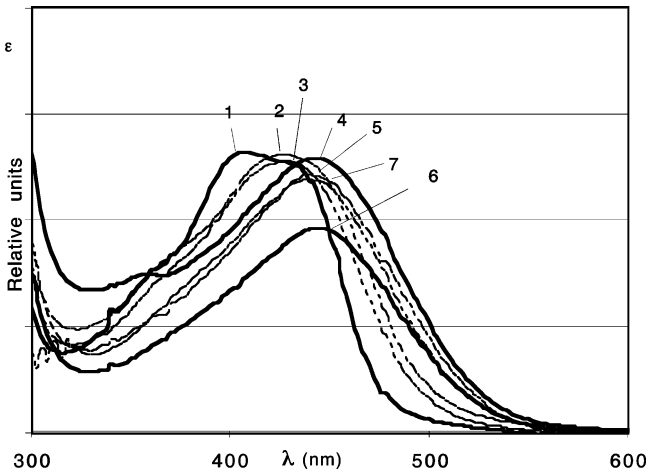

Figure 14. Plot of the low-energy transition for $(\eta^2\text{-dppe})(\eta^5\text{-}C_5Me_5)Fe(C{\equiv}C)\text{-}1,4\text{-}(C_6H_4)CN$ (**1b**) in various solvents: (1) *n*-pentane; (2) toluene; (3) diethyl ether; (4) dichloromethane; (5) acetone; (6) acetonitrile; (7) methanol.

Phenomenological Approach of the Electronic Substituent Effect in Fe(II) Acetylides. Linear correlations found between redox potentials or characteristic spectroscopic data of the Fe−C≡C fragment and ESPs (Figures 9−11) for **1a**−**j**, here and in previous work,[1b] constitute unprecedented[21] observations for transition-metal acetylides.[43,44] Such LFERs provide information about the relative importance of π (mesomeric) vs σ (inductive) MO effects with respect to the transmission of the electronic influence between the X substituent and the aryl ring.[45,46]

1. Correlation of Hammett ESPs with the Fe(III)/Fe(II) Redox Potentials. The good correlation which is obtained (Figure 9) indicates that the substituent effect results from a balanced situation between π and σ effects.[44a−e] In classical LFERs, the nature of the ESPs is strongly connected to the ground state (GS) VB structure of the aryl ring bearing the X substituent in the reactant and product. Presently, the use of Hammett ESPs indicates that none of them does present a marked cumulenic character.[23] In agreement with previous suppositions,[1a] possible VB mesomers different from A

(42) Powell, C. E.; Cifuentes, M. P.; Morall, J. P.; Stranger, R.; Humphrey, M. G.; Samoc, M.; Luther-Davies, B.; Heath, G. A. *J. Am. Chem. Soc.* **2003**, *125*, 602−610.

(43) For selected LFERs on organic acetylenes, see: (a) Cook, C. D.; Danyluk, S. S. *Tetrahedron* **1962**, *19*, 177−185. (b) Charton, M. *J. Org. Chem.* **1972**, *37*, 3684−3687. (c) Eaborn, C.; Eastmond, R.; Walton, D. R. M. *J. Chem. Soc. B* **1971**, 127−130. (d) Eaborn, C.; Walton, D. R. M. *J. Organomet. Chem.* **1965**, *4*, 217−228. (e) Veschambre, H.; Dauphin, G.; Kergomard, A. *Bull. Soc. Chim. Fr.* **1967**, 2846−2854. (f) Veschambre, H.; Dauphin, G.; Kergomard, A. *Bull. Soc. Chim. Fr.* **1967**, 134−139.

(44) For selected LFERs on organometallic complexes, see: (a) Mason, J. G.; Rosenblum, M. *J. Am. Chem. Soc.* **1960**, *82*, 4206−4208. (b) Hoh, G. L. K.; MacEwen, W. E.; Kleinberg, J. *J. Am. Chem. Soc.* **1961**, *83*, 3949. (c) Gubin, S. P.; Perevalova, E. G. *Dokl. Chem.* **1962**, *143*, 346−349. (d) Little, W. F.; Reiley, C. N.; Johnson, J. D.; Lynn, K. N.; Sanders, A. P. *J. Am. Chem. Soc.* **1964**, *86*, 1376−1381. (e) Gubin, S. P.; Khandkarova, V. S. *J. Organomet. Chem.* **1970**, *22*, 449−460. (f) Müller, T. J. J.; Ansorge, M.; Lindner, H. J. *Chem. Ber.* **1996**, *129*, 1433−1440.

(45) March, J. *Advanced Organic Chemistry. Reactions, Mechanisms and Structures*, 4th ed.; Wiley: New York, 1992.

(46) Katritzky, A. R.; Topsom, R. D. *Angew. Chem., Int. Ed. Engl.* **1970**, *9*, 87−99.

Scheme 2

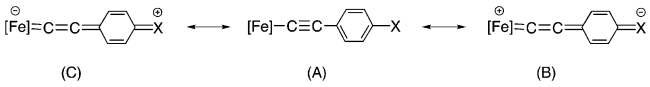

must therefore have only a small relative weight in the GS of most Fe(II) acetylides investigated here (Scheme 2).

Proceeding from eq 2 to a MO-based understanding of the electronic substituent effect is not straightforward.[47] In low symmetry (C_1) molecules such as **1a**−**j**, mixing between the π- and σ-type MO manifolds is allowed to some extent and the electronic perturbation induced by the X substituent is distributed over many MOs. An alternative attempt for relating such empirical correlations to the computed data relies on the postulate initially made by Hammett.[23,48] The latter states that the ESP values are proportional to the charge induced by the X substituent of the carbon atom bearing "the reacting site" relative to the unsubstituted molecule.[49,50] Owing to nodal properties of the HOMO in **1a**-H−**1j**-H, the "reacting site" for oxidation is mostly the whole (η^2-dppe)(C_5Me_5)Fe−C≡C fragment. We have therefore examined the changes in charge distribution in the Fe−C≡C−(C1) unit in the model complexes (Table 6). A very weak increase in negative charge takes place on iron (0.005 e) and on C_β (0.008 e) with electron-releasing substituents, but the trend is much more pronounced for C_α (0.022 e) and C1 (0.030 e). For these atoms, good linear correlations (see Supporting Information) are obtained between the Hammett ESPs and the Hirshfeld charges on Fe (R = 0.96), C_α (R = 0.96) and C1 (R = 0.98). Therefore, the substituent effects on the redox potentials in eq 2 can be understood as a *global* charge effect resulting from different polarizations of the complete Fe−C≡C side chain in Fe(II) complexes.[20b]

2. Correlation of ESPs with the Energy of the MLCT Absorption. Equation 3 shows the electronic influence of the X substituent on the energy of the optical transition between the ground state (GS) and the first excited state. In this correlation, mesomeric substituent effects appear to be predominant over the inductive effects, the best fit being achieved with the σ^- ESPs rather than with σ ESPs. Given the peculiar form of this LFER, substituent effects in both the *ground* and *excited* states are now reflected, in contrast to the previous situation (eq 2).[51] TD-DFT computations on **1a**-H−**1k**-H have established that this excitation does involve electrons which are promoted from MOs with a dominant metal character toward mostly phenylalkynyl-based MOs. Considering the large mesomeric influence of the substituent evidenced here, the VB formulation A*, analogous to B, could typically represent the excited MLCT state, especially for **1a** or **1b** (Scheme 3).[52] In accordance with the polar nature of such an excited state, we observe a weak but overall

Scheme 3

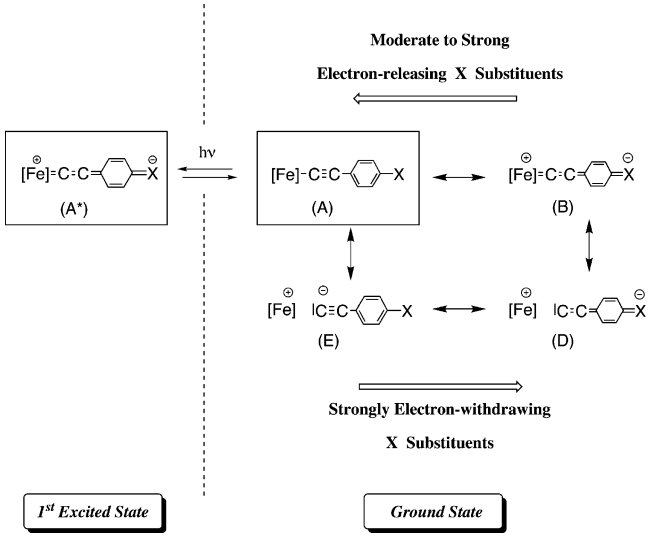

positive solvatochromy for this transition for **1a** (ca. 40 nm) and **1b** (≥10 nm; Figure 14).[53,54] A related EFISH study on **1a**−**k** strongly suggested that this first excited state plays a crucial role with respect to the second-order polarizability exhibited by the Fe−C≡C fragment in Fe(II) complexes, especially when electron-withdrawing substituents are tethered to the aryl ring.[1c] In terms of perturbational approach,[52] this means that a VB mesomer such as B increases its weight in the GS representation under the influence of an electromagnetic field. Conversely, this also indirectly evidences that this VB mesomer already has a small weight in the *unperturbed* GS of electron-rich Fe(II) acetylides such as **1a**−**k**.

3. Correlation of ESPs with the ^{13}C NMR Shift of the α-Carbon of the Acetylide Linker. The last correlation (eq 3) also involves spectroscopic data and clearly evidences the substituent influence on the ^{13}C NMR shifts of the α-carbon. For carbon atoms directly linked to a metal center, the so-called paramagnetic contribution to the shift (δ_{para}) is most often determinant[55] but difficult to calculate with accuracy, relying on a very accurate description of the excited state.[56] This paramagnetic contribution principally originates from the contribution of low-lying excited states, presenting a strong localization on the α-carbon atom. The low-lying MLCT state might therefore constitute an important contributor to the ^{13}C NMR shifts in **1a**−**k**. Accordingly, a crude correlation (R = 0.91) is observed between the ^{13}C NMR shifts and the wavelength of the first electronic transition (i.e. the MLCT).[57,58]

Alternatively, eq 3 also suggests that there might be a relationship between the charge distribution of the α-carbon induced by the substituent and its ^{13}C NMR shift for this series of Fe(II) acetylide complexes.[49,59]

(47) (a) Guérillot, C.-R. *J. Chim. Phys.* **1962**, *59*, 1039−1047. (b) Guérillot, C.-R. *J. Chim. Phys.* **1960**, *57*, 110−124.
(48) Hammett, L. P. *J. Am. Chem. Soc.* **1937**, *59*, 96−103.
(49) Topsom, R. D. *Acc. Chem. Res.* **1983**, *16*, 292−298.
(50) (a) Jaffé, H. H. *J. Am. Chem. Soc.* **1954**, *76*, 5843−5846. (b) Jaffé, H. H. *J. Chem. Phys.* **1952**, *20*, 279−284. (c) Jaffé, H. H. *J. Chem. Phys.* **1952**, *20*, 778−780.
(51) Ulman, A. *J. Chem. Phys.* **1988**, *92*, 2385−2390.
(52) Dehu, C.; Meyers, F.; Brédas, J. L. *J. Am. Chem. Soc.* **1993**, *115*, 6198−6206.
(53) Reichardt, C. *Chem. Rev.* **1994**, *94*, 2319−2358.
(54) No clear solvatochromy is observed for complexes such as **1g** containing more electron-releasing substituents (see the Supporting Information).
(55) Czech, P. T.; Ye, X.-Q.; Fenske, R. F. *Organometallics* **1990**, *9*, 2016−2022.
(56) Evans, J.; Norton, J. R. *Inorg. Chem.* **1974**, *13*, 3042−3043.
(57) Sebald, A.; Wrackmeyer, B.; Beck, W. *Z. Naturforsch.* **1983**, *38b*, 45−56.
(58) Connor, J. A.; Jones, E. M.; Randall, E. W.; Rosenberg, E. *J. Chem. Soc., Dalton Trans.* **1972**, 2419−2424.

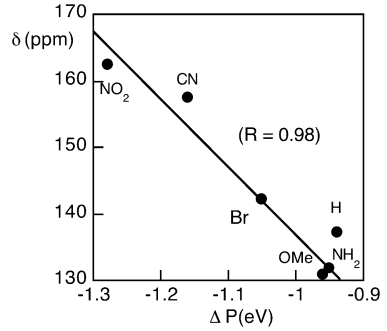

Figure 15. Plot of the alkynyl ^{13}C NMR C_α shifts (ppm) in (η^2-dppe)(η^5-C_5Me_5)Fe(C≡C)-1,4-(C_6H_4)X complexes vs the ΔP (=$\Delta E\pi_{M\rightarrow L} - \Delta E\pi_{L\rightarrow M}$) difference (eV) computed for the Fe−C heterolytic BDE in the corresponding model complexes (X = NO_2, CN, Br, H, OMe, NH_2).

This assumption is supported by the good linear correlation ($R = 0.99$) observed between the ^{13}C NMR shift of the α-carbon in **1a**−**j** and the Hirshfeld charge computed for the corresponding model complexes **1a**-H−**1j**-H. In **1a**−**k**, the α-carbon atom is π-conjugated with the aryl *p*-X carbon, resulting in a charge dependence between these centers, as expected from the alternant nature of the arylethynyl ligand. Considering that the ^{13}C NMR shifts for most aromatic compounds are determined by the paramagnetic term[60,61] which also depends on the local atomic charge, in particular that of π-type,[62−64] we believe likewise that local changes in charge are important in determining the shift of the α-carbon for **1a**−**j**. In this connection, recent NBO calculations of Low and co-workers on **3a**−**c** show that π charges are much more affected than σ charges by a change of the X substituent.[20b] Our calculations on **1a**-H−**1j**-H do not provide an easy access to local π charges on the α-acetylide carbon; however, the decisive role of local π charge polarization is revealed when these ^{13}C NMR shifts are plotted vs the difference between the $\Delta E\pi_{M\rightarrow L}$ and $\Delta E\pi_{L\rightarrow M}$ terms previously determined for the heterolytic Fe−C BDE (Table 7). Indeed, considering that $\Delta E\pi_{M\rightarrow L}$ and $\Delta E\pi_{L\rightarrow M}$ are related to the weights of the VB isomers B and C, respectively (Scheme 2), the difference (ΔP) between these terms should reflect the π polarization at the α-carbon atom. A good correlation is obtained, especially when the data for the unsubstituted (X = H) complex **1f** are not included (Figure 15). The downfield ^{13}C NMR shift of the α-carbon in **1a**−**j** might therefore reflect the "cumulenic" character induced by a given substituent, i.e. resulting from the balance between back- and forward-bonding, or between formulas B and C in terms of VB description (Scheme 2).[63a,65−67] Accordingly, the ^{13}C NMR signals for the α-carbon atom in carbene or cumulene complexes are strongly deshielded relative to those of related alkynyl complexes.[22a,68,69]

Valence Bond (VB) Representation of the Ground State (GS) for Electron-Rich Fe(II) Acetylides. DFT computations on **1a**-H−**1j**-H and LFERs confirm that **1a**−**k** are mostly described by the VB formula A in the GS, the weight of other VB contributors remaining weak (Scheme 3).[1a,b] Among the various polar structures previously envisioned to rationalize π-interactions which emphasize the role of the metal fragment as electron donor, such as B/B_1 in Scheme 1 or B′/B″ given below,[1b]

(B′) (B″)

we favor B, since it presents main-group atoms which obey the octet rule. Furthermore, as pointed out previously, the weight of this VB mesomeric form in the GS certainly increases when compounds containing electron-withdrawing substituents are placed in an electromagnetic field (Scheme 3).[1c] In addition to B, the DFT computations suggest also the participation of ionic structures such as D and E. Indeed, in comparison to metal acetylides such as **2**, these VB structures reflect the strong ionic character of the metal−acetylide interaction in electron-rich Fe(II) complexes such as **1h**. Thus, D explains more specifically the decrease in Fe−C heterolytic BDE with electron-withdrawing substituents, whereas E rationalizes the presence of negative charge density on the α-alkynyl carbon atom with electron-releasing substituents in the GS, which is not explained by B alone (Scheme 4). A close examination of charge distribution reveals that the positive fractional charge on the $[Fe]^+$ fragment due to B, D, and E is actually distributed over the phosphorus atoms rather than localized at the iron nucleus, as already stated for **3a**−**c**.[20b] In Scheme 3, the VB structure D counteracts to some extent the increase in metal−carbon bond order induced by π-interactions (B), which would explain the relative constancy of the Fe−C bond distance observed experimentally in many Fe(II) representatives (Table 3). The canonical structures B, D, and E have similar influences with respect to the direction and magnitude of the molecular dipole moments in the GS[1b] and are possibly at the origin of the strong influence of σ-inductive/polar effects exerted by the alkynyl ligand on the first ionization potential.[19a,20b,41]

Conclusions. The combined theoretical/phenomenological approach carried out here fully establishes the good electronic communication existing between the iron center and the X substituent through the phenylalkynyl linker in complexes **1a**−**j.** The substituent effect can be understood in terms of changes in charge distribution within the Fe−C≡C fragment. This contribution also points out the decisive importance of π-interactions with respect to the spectroscopic properties of electron-rich Fe(II) alkynyls. Notably, iron-to-alkynyl back-bonding

(59) Chapman, N. B.; Shorter, J. *Advances in Linear Free Energy Relationships*; Plenum Press: London, 1972.
(60) Rosenberg, D.; Drenth, W. *Tetrahedron* **1971**, *27*, 3893−3907.
(61) Mason, J. *J. Chem. Soc. A* **1971**, 1038−1047.
(62) Bloor, J. E.; Breen, D. L. *J. Phys. Chem.* **1968**, *72*, 716−722.
(63) (a) Bromilow, J.; Brownlee, R. T. C.; Craik, D. J.; Sadek, M.; Taft, R. W. *J. Org. Chem.* **1980**, *45*, 2429−2438. (b) Bromilow, J.; Brownlee, R. T. C.; Lopez, V. O.; Taft, R. W. *J. Org. Chem.* **1979**, *45*, 2429−2438.
(64) Maciel, G. E.; Natterstad, J. J. *J. Chem. Phys.* **1965**, *42*, 2427−2435.
(65) Olah, G. A.; Spear, R. J.; Westerman, P. W.; Denis, J.-M. *J. Am. Chem. Soc.* **1974**, *96*, 5855−5859.
(66) Whittall, I. R.; Humphrey, M. G.; Hockless, D. C. R.; Skelton, B. W.; White, A. H. *Organometallics* **1995**, *14*, 3970−3979.
(67) Akita, M.; Chung, M.-C.; Terada, M.; Miyauti, M.; Tanaka, M.; Moro-oka, Y. *J. Organomet. Chem.* **1998**, *565*, 49−62.
(68) Coat, F.; Guillemot, M.; Paul, F.; Lapinte, C. *J. Organomet. Chem.* **1999**, *578*, 76−84.
(69) Connelly, N. G.; Gamasa, M. P.; Gimeno, J.; Lapinte, C.; Lastra, E.; Maher, J. P.; Le Narvor, N.; Rieger, A. L.; Rieger, P. H. *J. Chem. Soc., Dalton Trans.* **1993**, 2575−2578.

was evaluated. Although weak on average, this stabilizing π-interaction increases with electron-withdrawing substituents to become more and more influential. From a VB point of view, the series of Fe(II) acetylides **1a**−**j** should not depart significantly from the typical alkynyl structure A in the ground state (Scheme 3). Nevertheless, strong electron-withdrawing substituents can induce a sizable polarization of the π-manifold, represented by the structure B. In addition, as pointed out by the present work, the iron−alkynyl bonding presents also a non-negligible ionic character, exemplified by VB structures D and E. Finally, the electronic structure of the stable and isolable Fe(III) redox parents **1a**$^+PF_6^-$ through **1j**$^+PF_6^-$ was also briefly investigated. The data reveal that only slight structural modifications take place upon oxidation, regardless of the X substituent, and suggest that the inner contribution to the reorganization energy (λ_{in}) will also remain weak for the redox-active (η^2-dppe)(η^5-C_5Me_5)Fe(C≡C)-1,4-(C_6H_4)− fragment in larger molecular assemblies.

Experimental Section

Computational Details. DFT calculations were carried out using the Amsterdam Density Functional (ADF) program.[70,71] The model compounds Fe(η^5-C_5H_5)(PH_3)$_2$(*p*-C_6H_4X)$^{n+}$ (X = NO_2, CN, H, OMe, NH_2; n = 0, 1) were used in order to reduce computational effort. Electron correlation was treated within the local density approximation (LDA) in the Vosko−Wilk−Nusair parametrization.[72] The nonlocal corrections of Becke[73] and Perdew[74] were added to the exchange and correlation energies, respectively. The numerical integration procedure applied for the calculations was developed by te Velde et al.[70] The basis set used for the metal atoms was a triple-ζ Slater-type orbital (STO) basis for Fe 3d and 4s and a single-ζ function for Fe 4p. A triple-ζ STO basis set was employed for H 1s and for 2s and 2p of C, N, and O, extended with a single-ζ polarization function (2p for H; 3d for C, N, and O) for X groups. The valence orbitals of the atoms of the other groups (C_5H_5, PH_3) were described by a double-ζ STO basis set. Full geometry optimizations (assuming C_1 symmetry) were carried out on each complex, using the analytical gradient method implemented by Verluis and Ziegler.[75] Spin-unrestricted calculations were performed for all the considered open-shell systems. Time-dependent density functional theory (TD-DFT) calculations were performed on the optimized structures of the Fe(II) series employing the same functional and basis set than described above.[76] The excitation energies and oscillator strengths were calculated by following the procedure described by van Gisbergen and co-workers.[76]

Most of the theoretical data were obtained from optimized conformations in which the phenyl plane is roughly parallel to the C_5Me_5 plane. However, the energy difference between conformers where the metal fragment is rotated around the Fe−C bond is less than 0.5 kcal/mol (0.3 and 0.4 kcal for X = NO_2, NH_2, respectively, for a 90° rotation). Finally, to evaluate the approximation made when using hydrogen-substituted model complexes, the electronic structure of complex **1a** was theoretically computed and compared to that obtained of **1a-H**. Similar results were obtained. This gave confidence in results obtained for the model complexes **1a-H**−**1j-H**.

Decomposition of the Fe−C_α interaction energy was done according to the *transition state* method of Ziegler and Rauk. In this method, the interaction energy can be split up into different physically meaningful terms: $\Delta E = \Delta E_{el} + \Delta E_{orb} + \Delta E_{Pauli}$. ΔE_{el} is the classical electrostatic interaction between the charge distributions of the interacting fragments in their unrelaxed geometry and is generally attractive (>0). ΔE_{Pauli} roughly corresponds to the energy issued of the interaction between the occupied orbitals of the fragments. ΔE_{orb} mainly accounts for the interaction between occupied and vacant orbitals. The latter can be decomposed into σ and π (parallel and perpendicular to the plane of the phenyl ring) components, which were calculated using the procedure implemented in the ADF code: $\Delta E_{orb} = \Delta E\sigma + \Delta E\pi_{M\rightarrow L} + \Delta E\pi_{L\rightarrow M}$. Optimized geometries with C_s symmetry were used.[30,31] The latter were calculated not to be more than 1 kcal/mol less stable than the fully optimized systems, with the exception of that containing the substituent X = OMe. In that particular case, imposing C_s symmetry consists of rotating the OMe substituent by 90° (OMe plane perpendicular to the phenyl ring), which is quite destabilizing (4.1 kcal/mol). Representation of the molecular orbitals was done using MOLEKEL4.1.[77]

Crystallography. Crystals of **1e**,**g**,**i**,**j** were obtained by slow evaporation of a solution of the complexes under argon in diethyl ether (**1e**,**g**), $CHCl_3$ (**1i**), or C_6H_6 (**1j**). The samples were studied on a NONIUS Kappa CCD with graphite-monochromated Mo Kα radiation. The cell parameters were obtained with Denzo and Scalepack with 10 frames (ψ rotation: 1° per frame).[78] Data collection[79] ($2\theta_{max}$, number of frames, ω rotation, seconds per frame, and *hkl* range as given in Table 1) gives 22 360, 25 985, 39 160, and 29 159 reflections for **1e**,**g**,**i**,**j**, respectively. Data reduction with Denzo and Scalepack[78] gave the independent reflections (Table 1). The structures were solved with SIR-97, which reveals the non-hydrogen atoms.[80] After anisotropic refinement, the remaining atoms were found by a Fourier difference map. The whole structures were then refined with SHELXL-97[81] by full-matrix least-squares techniques (use of F^2 magnitude; x, y, z, β_{ij} for Fe, P, C, N, and/or O atoms, x, y, z in riding mode for H atoms with variables "N(var.)", observations, and "w" used as defined in Table 1).

Atomic scattering factors were taken from the literature as given in the manual for SHELXL-97.[82] ORTEP views of **1e**,**g**,**i**,**j** were realized with PLATON98.[83] All the calculations were performed on a Pentium NT Server computer.

Acknowledgment. The CNRS is acknowledged for financial support. We thank the Centre de Ressources Informatiques (CRI, Rennes, France) and the Institut de Développement et de Ressources en Informatique (IDRIS, Orsay, France) for computing facilities.

(70) (a) te Velde, G.; Bickelhaupt, F. M.; Fonseca Guerra, C.; van Gisbergen, S. J. A.; Baerends, E. J.; Snijders, J.; Ziegler, T. *Theor. Chim. Acta* **2001**, *22*, 931−967. (b) Fonseca Guerra, C.; Snijders, J.; te Velde, G.; Baerends, E. J. *Theor. Chim. Acta* **1998**, *99*, 391−403.

(71) ADF2002.01; Theoretical Chemistry, Vrije Universiteit, Amsterdam, The Netherlands, SCM.

(72) Vosko, S. D.; Wilk, L.; Nusair, M. *Can. J. Chem.* **1990**, *58*, 1200−1211.

(73) (a) Becke, A. D. *J. Chem. Phys.* **1986**, *84*, 4524−4529. (b) Becke, A. D. *Phys. Rev. A* **1988**, *38*, 3098−3100.

(74) (a) Perdew, J. P. *Phys. Rev. B* **1986**, *33*, 8822−8824. (b) Perdew, J. P. *Phys. Rev. B* **1986**, *34*, 7406-.

(75) Verluis, L.; Ziegler, T. *J. Chem. Phys.* **1988**, *88*, 322−328.

(76) van Gisbergen, S. J. A.; Snijders, J. G.; Baerends, E. J. *J. Comput. Phys. Commun.* **1999**, *118*, 119.

(77) Flükiger, P.; Lüthi, H. P.; Portmann, S.; Weber, J. Swiss Center for Scientific Computing (CSCS), 2000−2001.

(78) Otwinowski, Z.; Minor, W. In *Methods in Enzymology*; Carter, C. W., Sweet, R. M., Eds.; Academic Press: London, 1997; Vol. 276, pp 307−326.

(79) Kappa CCD Software; Nonius BV, Delft, The Netherlands, 1999.

(80) Altomare, A.; Burla, M. C.; Camalli, M.; Cascarano, G.; Giacovazzo, C.; Guagliardi, A.; Moliterni, A. G. G.; Polidori, G.; Spagna, R. *J. Appl. Chem.* **1998**, *31*, 74−77.

(81) Sheldrick, G. M. SHELX97-2: Program for the Refinement of Crystal Structures; University of Göttingen, Göttingen, Germany, 1997.

(82) Reidel, D. *International Tables for Crystallography*; Wilson, A. J. C., Ed.; Kluwer Academic: Dordrecht, The Netherlands, 1992; Vol. C.

(83) Spek, A. L. PLATON: A Multipurpose Crystallographic Tool; Utrecht University, Utrecht, The Netherlands, 1998.

Supporting Information Available: Tables of ESPs, tables of electrochemical data for **1a**−**j**, figures giving the solvatochromy of the MLCT absorption for complex **1g**, a detailed table of orbital contributions for the heterolytic BDE of the Fe−C bond in **1a**-H−**1j**-H, plots of computed IPs or Hirshfeld charges (for selected atoms) vs Hammett ESPs, plots of the ^{13}C NMR shift of C_α vs the Hirschfeld charge computed, and X-ray structural information for **1e**,**g**,**i**,**j**, including tables of atomic positional parameters, bond distances and angles, and anisotropic and isotropic thermal displacement parameters.This material is available free of charge via the Internet at http://pubs.acs.org.

OM030630K